Journal of Volcanology and Geothermal Research xxx (2016) xxx–xxx

Contents lists available at ScienceDirect

Journal of Volcanology and Geothermal Research

journal homepage: www.elsevier.com/locate/jvolgeores

Morphologic and thermophysical characteristics of lava flows southwest of Arsia Mons, Mars

David A. Crown [a,*], Michael S. Ramsey [b]

[a] Planetary Science Institute, 1700 E. Fort Lowell Road, Suite 106, Tucson, AZ 85719, United States
[b] Department of Geology and Planetary Science, University of Pittsburgh, 4107 O'Hara Street, Room 200, Pittsburgh, PA 15260, United States

ARTICLE INFO

Article history:
Received 12 October 2015
Received in revised form 9 May 2016
Accepted 24 July 2016
Available online xxxx

Keywords:
Lava flows
Arsia Mons
Tharsis region
Remote sensing
Thermophysical

ABSTRACT

The morphologic and thermophysical characteristics of part of the extensive lava flow fields southwest of Arsia Mons (22.5–27.5°S, 120–130°W) have been examined using a combination of orbital VNIR and TIR datasets. THEMIS images provide context for the regional geology and record diurnal temperature variability that is diverse and unusual for flow surfaces in such close proximity. CTX images were used to distinguish dominant flow types and assess local age relationships between individual lava flows. CTX and HiRISE images provide detailed information on flow surface textures and document aeolian effects as they reveal fine-grained deposits in many low-lying areas of the flow surfaces as well as small patches of transverse aeolian ridges. Although this region is generally dust-covered and has a lower overall thermal inertia, the THEMIS data indicate subtle spectral variations within the population of lava flows studied. These variations could be due to compositional differences among the flows or related to mixing of flow and aeolian materials. Specific results regarding flow morphology include: a) Two main lava flow types (bright, rugged and dark, smooth as observed in CTX images) dominate the southwest Arsia Mons/NE Daedalia Planum region; b) the bright, rugged flows have knobby, ridged, and/or platy surface textures, commonly have medial channel/levee systems, and may have broad distal lobes; c) the dark, smooth flows extend from distributary systems that consist of combinations of lava channels, lava tubes, and/or sinuous ridges and plateaus; and d) steep-sided, terraced margins, digitate breakout lobes, and smooth-surfaced plateaus along lava channel/tube systems are interpreted as signatures of flow inflation within the dark, smooth flow type. These flows exhibit smoother upper surfaces, are thinner, and have more numerous, smaller lobes, which, along with their the channel-/tube-fed nature, indicate a lower viscosity lava than for the bright, rugged flows. Flow patterns and local interfingering and overlapping relationships are delineated in CTX images and allow reconstruction of the complex flow field surfaces. Darker channel-/tube-fed flows are generally younger than adjacent thicker, bright, rugged flows; however, the diversity and complexity of temporal relationships observed, along with the thermophysical variability, suggests that lava sources with different eruptive styles and magnitudes and/or lavas that experienced different local emplacement conditions were active contemporaneously.

1. Introduction

The acquisition of high spatial resolution datasets with significant areal coverage provides an opportunity to explore the styles, magnitudes, and sequences of Martian volcanism in detail. The current investigation uses visible/near-infrared (VNIR) and thermal infrared (TIR) imaging to characterize lava flow fields of southern Tharsis, specifically those southwest of Arsia Mons and farther to the south in Daedalia Planum. Arsia Mons, the southernmost of the prominent Tharsis shield volcanoes, exhibits well-developed lava flow fields with a multitude of individual flows and flow lobes. Recent orbital data of the Martian surface now reveal small-scale characteristics of lava flow surfaces that provide new insights into the flow emplacement processes responsible for their formation. Our research examines flow morphology, local sequences of flow emplacement and flow field stratigraphy, degradation of flow field surfaces, and the unusual thermophysical variability of this flow field. The region includes lava flows that have been shown to exhibit some of the roughest surfaces on Mars at centimeter-to-meter-scales (Bandfield, 2009), as well as flows in close proximity showing all four types of diurnal temperature response (i.e., cool or warm in the day and cool or warm at night, as well as both kinds of day/night temperature inversions (Ramsey and Crown, 2010)). The region generally has a moderate overall dust cover and relatively low nighttime thermal inertia. Therefore, these diurnal temperature variations are likely caused by a complex combination of dust cover, albedo,

* Corresponding author.
E-mail addresses: crown@psi.edu (D.A. Crown), mramsey@pitt.edu (M.S. Ramsey).

http://dx.doi.org/10.1016/j.jvolgeores.2016.07.008

Please cite this article as: Crown, D.A., Ramsey, M.S., Morphologic and thermophysical characteristics of lava flows southwest of Arsia Mons, Mars, J. Volcanol. Geotherm. Res. (2016), http://dx.doi.org/10.1016/j.jvolgeores.2016.07.008

and surface roughness. Thermal infrared datasets are also used to evaluate potential spectral differences and interpret physical properties of surface materials. Our combined morphologic and thermal characterization of this region is important both for interpreting the styles and diversity of Martian volcanism and for extending detailed thermal infrared analyses to comparable areas of the Martian surface.

2. Study area

Arsia Mons along with Pavonis and Ascraeus Montes form a linear chain of three large shield volcanoes that, along with Olympus Mons to the northwest, dominate the Tharsis volcanic province on Mars. Arsia Mons is 461 × 326 km across and 17.7 km high, with exposed relief of 11 + km (relative to the Tharsis plateau) and flank slopes averaging ~5° (Plescia, 2004). Daedalia Planum is an elevated plains region at the southern margin of the Tharsis province, where lava flows and plains embay remnants of highland terrain (e.g., Scott and Tanaka, 1986; Dohm et al., 2001). Typical surface slopes of the lava flow fields decrease steadily from 0 to 5° south of Arsia Mons to <0.5° at the southern margin of Daedalia Planum (Crown et al., 2012).

Arsia Mons has a well-developed summit caldera (Crumpler and Aubele, 1978; Crumpler et al., 1996; Head et al., 1998a, 1998b; Mouginis-Mark, 2002) and exhibits two large flow aprons that extend from alcoves on its northeast and southwest flanks and postdate its main shield (Plescia, 2004; Scott and Zimbelman, 1995; Bleacher et al., 2007a; Garry et al., 2014). The current investigation focuses on a zone (22.5–27.5°S, 120–130°W) (Fig. 1) within the extensive flow fields southwest of Arsia Mons and in northeast Daedalia Planum, for which high-resolution (1–15 m) VNIR and moderate-resolution (100 m) TIR data coverage is available. This work is part of broader studies of the southern Tharsis region of Mars that include geologic/flow field mapping (Crown et al., 2009, 2010, 2011, 2012, 2013, 2015, 2016, in preparation; Crown and Berman, 2012; Chuang et al., 2016; Crown, 2016, in preparation) and thermophysical mapping and modeling (Ramsey and Crown, 2010; Ramsey et al., 2012; Price et al., 2013; Simurda et al., 2015) to document the volcanic evolution of Mars' largest volcanic province.

3. Previous work

Using Viking Orbiter images, a series of sixteen 1:2 M scale lava flow maps were previously completed for the Tharsis region. Our study examines lava flows in what were defined as the Tharsis Montes and Arsia Mons flow units (Scott, 1981; Scott and Tanaka, 1981; Scott et al., 1981). Lava flows have long been recognized to the southwest of Arsia Mons, and the morphologic properties of individual flows as documented in Viking Orbiter images were used to provide some of the earliest estimates of rheologic properties of Martian lavas (Moore et al., 1978; Schaber et al., 1978). Warner and Gregg (2003) used Mars Orbiter Camera (MOC) images to document the ridged surface texture exhibited by lava flows southwest of Arsia Mons and made measurements of flow properties (e.g., flow dimensions, ridge spacing and amplitude) to estimate rheologic parameters that were consistent with basaltic or basaltic andesite compositions. More recent studies of the Tharsis region have utilized Mars Express High Resolution Stereo Camera (HRSC) images to identify small vents and their associated flow fields, to distinguish different flow morphologies, and to examine evolutionary stages in effusive volcanism (Bleacher et al., 2007a,b; see

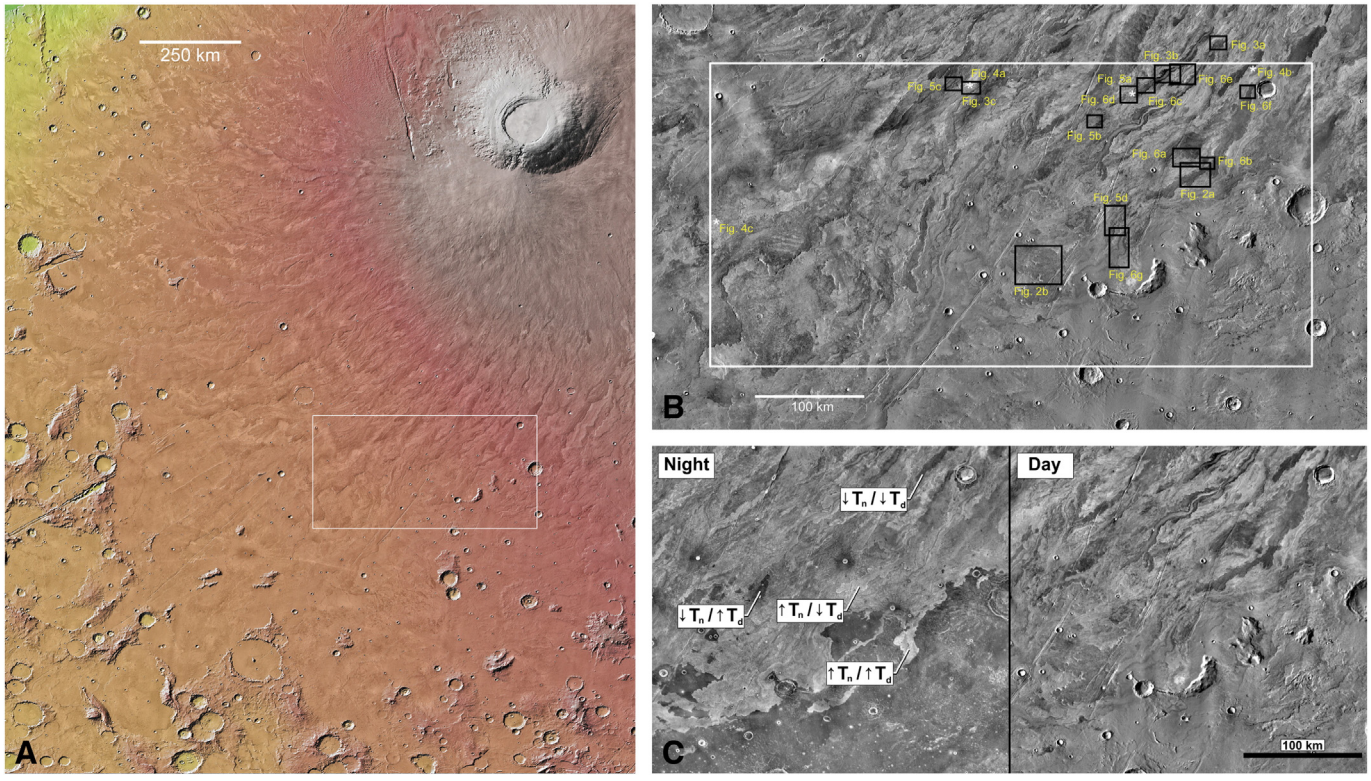

Fig. 1. A. MOLA color hill shade image (illuminated from the NW) showing location of the southwest Arsia Mons flow field study area (22.5–27.5°S, 120–130°E) outlined by white box (see Crown et al., 2015; Crown, 2016, in preparation). Note the Arsia Mons edifice (upper right) with summit caldera, southwest apron, and surrounding flow fields; remnants of ancient cratered terrain to south and southwest are embayed by southern Tharsis lava flows. North is to the top in this and all other figures. B. THEMIS TIR daytime image mosaic showing the Arsia Mons flow field study area (22.5–27.5°S, 120–130°W) outlined by white box. Locations of Figs. 2–6 are indicated by black boxes and white asterisks. C. Comparison of THEMIS TIR nighttime and daytime mosaics for the eastern part of the southwest Arsia Mons flow field, showing unusual variations in diurnal thermophysical behavior of the flows. T_n and T_d refer to the nighttime and daytime temperatures, respectively, and the arrows indicate cooler (down) and warmer (up) temperatures. Note that all possible combinations of day-night temperature variations are observed in relatively close proximity to one another.

Please cite this article as: Crown, D.A., Ramsey, M.S., Morphologic and thermophysical characteristics of lava flows southwest of Arsia Mons, Mars, J. Volcanol. Geotherm. Res. (2016), http://dx.doi.org/10.1016/j.jvolgeores.2016.07.008

also Bleacher et al., this volume). Zones dominated by different flow types were documented on the southern flanks of Arsia Mons and in the Arsia rift apron at the southern base of the edifice (north of the present study area); the most abundant volcanic units in this area were mottled, hummocky, channel-fed flows, and tube-fed flows. Comparisons have also been made between the thermal infrared spectral signatures of SNC meteorites and those of relatively dust-free lava flows in Daedalia Planum to the south of the current study area which show consistency with the basaltic shergottites (Lang et al., 2009).

Giacomini et al. (2009) used Thermal Emission Imaging System (THEMIS) and Mars Orbiter Laser Altimeter (MOLA) data to produce a map of lava flow units in Daedalia Planum (south of the present study area) and categorized flows based on interpretations of stratigraphic relations and surface texture. They noted the presence of small features on flow surfaces that they attributed to flow inflation, including tumuli, lava rises, and squeeze-ups. Giacomini et al. (2012) examined flow morphologies and spectral characteristics in Daedalia Planum using THEMIS, HiRISE, and OMEGA data to investigate compositional properties and relationships to flow characteristics. They noted a general progression from older, broad flows with platy-ridged surface textures to younger, elongate flows with channels, as well as some cases where spectral behavior appeared to correlate with flow properties. Analysis of OMEGA data showed spectral signatures indicative of mafic minerals and consistent with tholeiitic basalts.

Ramsey and Crown (2010) showed that lava flows southwest of Arsia Mons (near 22.5°S, 238.0°E) have unusual thermophysical variability at the spatial scale of individual flow units. Geologic mapping suggests that some flows in this area are relatively young (~100 My) (Crown et al., 2011, 2015), which together with the observed thermophysical variability, reinforces the finding from Bandfield (2009) that this region has some of the greatest centimeter-to-meter-scale roughness on Mars. This roughness would be expected to decrease over time with continued erosion and aeolian mantling. Prior analyses of CTX and HiRISE images indicate that lava flows here are in fact partially mantled by aeolian infill (Crown et al., 2009). Thermal Emission Spectrometer (TES) and THEMIS-derived thermal inertia and visible albedo values indicate that a moderate amount of dust cover must be present in this region (Ruff and Christensen, 2002). Despite the complications of aeolian infilling and dust mantling, Ramsey and Crown (2010) identified thermal IR spectral variations between and along lava flows, as well as every style of albedo/thermophysical variability at the individual flow scale (see also Simurda et al., 2015). Diurnal temperature changes are expected for rocky surfaces that are free of dust (e.g., warm at night and cooler in the day relative to their surroundings) or those well-covered with dust (e.g., cool at night and warmer in the day) relative to other flows and surfaces in the region. However, some flows in this region show no temperature inversion between day and night in TIR data. Therefore, the overall complexity in thermal behavior at the scale of individual flows within the same geographic region is the likely result of an albedo-dominated influence of radiant temperature combined with the presence of variable amounts of surface dust and aeolian infill. These preliminary observations are expanded upon below as part of this systematic investigation of lava flow fields southwest of Arsia Mons.

In conjunction with geologic mapping of southern Tharsis including the southwest Arsia Mons and Daedalia Planum flow fields (Crown et al., 2009, 2010, 2011, 2012, 2013, 2015; Crown and Berman, 2012; Chuang et al., in review), Crown et al. (2015) derived age estimates for individual lava flows using CTX images from measured populations of small impact craters superposed on exposed lava flow surfaces. Results indicate an extensive history of volcanism across southern Tharsis. Crater size-frequency distributions for a series of elongate flow lobes south of Arsia Mons (including both the bright, rugged and dark, smooth flow types described below) indicate ages of ~100 My (Late Amazonian Epoch). Crater size-frequency distributions for adjacent broad flow lobes and for sheet flows farther southwest in Daedalia Planum indicate ages ~1+ Gy (Middle to Early Amazonian), with older volcanic plains exposed beneath the sheet flows at the southern margin of Tharsis. These age constraints are consistent with those found for lava flows in various locations across southern Tharsis by Holmok (2012) and Kapannusch (2012) using THEMIS and CTX images. Giacomini et al. (2009) report an age of 260 ± 90 My for the youngest flow in their Daedalia Planum study region using a HiRISE image. These chronologic results suggest a general decrease in age toward the center of Tharsis and that distinct sequences of flow emplacement may have characterized the Amazonian volcanic history of southern Tharsis.

4. Datasets

For analyses of southern Tharsis lava flow fields, we use a combination of VNIR and TIR imaging datasets, including 1) Mars Reconnaissance Orbiter (MRO) ConTeXt Camera (CTX; ~5 m/pixel) VNIR images, 2) MRO High Resolution Imaging Science Experiment (HiRISE; 0.25 m/pixel) VNIR images, 3) the Mars Odyssey THEMIS global mosaic (TIR brightness temperature) and individual daytime and nighttime TIR multi-band images (~100 m/pixel), and 4) the THEMIS-derived global thermal inertia mosaic (http://astrogeology.usgs.gov/maps/mars-themis-derived-globalthermal-inertia-mosaic). Images were imported into ArcGIS for flow lobe and flow field analyses in conjunction with related geologic and flow field mapping studies in southern Tharsis. A detailed discussion of THEMIS IR data and its use in this project follows.

The THEMIS IR imager consists of a 320 by 240 array of uncooled microbolometer detectors with 10 spectral channels centered between 6.8 and 14.8 μm with a spatial resolution of approximately 100 m/pixel (Bandfield et al., 2004; Christensen et al., 2004). THEMIS data have been composited into global mosaics of daytime and nighttime temperature as well as derived nighttime thermal inertia (Fergason et al., 2006; Edwards et al., 2011). Both are useful for visual and quantitative interpretations over large geographic areas. It was in these mosaic datasets that the unusual thermophysical properties of the study area were first observed (Ramsey and Crown, 2010). In addition, we analyzed two individual THEMIS IR daytime images (I07370003 and I43297003) covering lava flows in the study area. These were selected because they were acquired during periods of warmer daytime surface temperature due either to the season or a shift to an earlier equatorial crossing time by the Mars Odyssey spacecraft. The warmer surface temperatures resulted in data with a higher signal to noise ratio (SNR). Each IR dataset was acquired with all 10 bands, minimal atmospheric dust opacity, and local times between approximately 15:00 and 17:00.

Individual THEMIS IR radiance data are commonly corrected for atmospheric attenuation using the in-scene methodology of Bandfield et al. (2004), which relies upon previously-acquired TES data over the same area. A morphologically bland and spectrally homogeneous region of a few hundred pixels is chosen within the THEMIS IR scene at approximately the same surface elevation as the region of interest. The mean emissivity value is then extracted over this region for each IR channel. Atmospherically corrected TES data (bands 9–35 and 65–110) over that same region are also extracted, averaged together, and convolved to the THEMIS spectral response functions. Finally, THEMIS-derived emissivity values are divided by the TES-derived emissivity values for each band to derive an atmospheric correction scaling factor, which is then applied to the entire THEMIS emissivity dataset. Channels 1 and 2 (6.78 μm) are averaged together for better signal to noise, and channel 10 (14.88 μm) is removed due to the high atmospheric opacity, resulting in eight usable IR channels for surface observations. Once corrected for instrument calibration and atmospheric effects, the radiance-at-ground data are separated into brightness temperature and apparent surface emissivity using a normalized emissivity approach with an assumed maximum emissivity of 0.988 (Christensen, 1982; Realmuto, 1990).

Please cite this article as: Crown, D.A., Ramsey, M.S., Morphologic and thermophysical characteristics of lava flows southwest of Arsia Mons, Mars, J. Volcanol. Geotherm. Res. (2016), http://dx.doi.org/10.1016/j.jvolgeores.2016.07.008

5. Results: lava flows southwest of Arsia Mons

The following sections describe the results of our analyses of the lava flow fields southwest of Arsia Mons and in northeast Daedalia Planum, including descriptions of the main lava flow types and their morphologic characteristics, interactions between lava flows and flow field stratigraphy, and thermophysical variations that help to characterize the properties of flow surfaces.

5.1. Lava flow types and morphologic characteristics

It was clear from Mariner 9 and Viking Orbiter images that vast lava flow fields dominated the region to the southwest of Arsia Mons and formed the surface units in Daedalia Planum (e.g., Scott, 1981; Scott et al., 1981; Scott and Tanaka, 1981, 1986; Scott and Zimbelman, 1995). In some cases, individual lava flows were identified and traced (at least in part) in regional image mosaics; however, we now know from examination of more recent high-resolution imaging datasets that the flows evident in those early datasets are only a small fraction of the multitude that can be studied with currently available data. Furthermore, because the flows identified in those earlier studies were only the largest and most prominent flow lobes, they no longer provide an accurate representation of the nature and diversity of volcanism in this region. Details of flow surface morphology were illustrated in scattered high-resolution Viking Orbiter and MOC images, but without geologic and volcanic context from more systematic areal coverage, it was difficult to properly extrapolate from those views.

The THEMIS IR mosaic (initially at 230 m/pixel and now at ~100 m/pixel) and CTX image coverage now permit systematic and detailed analyses of the southern Tharsis lava flow fields. The higher (and more consistent) spatial resolution and greater dynamic range of the thermal infrared data allow for significantly improved delineation of individual lava flows. For example, the thermophysical properties exhibited by lava flows southwest of Arsia Mons reveal flow margins and central channels that were not clearly observed in Viking Orbiter images. CTX images (~5 m/pixel) allow improved discrimination of lobes as well as channel and levee structure, consistently revealing complex flow patterns and local interfingering and overlapping relationships across much of the region, as well as details of the flow surface morphology (e.g., Crown et al., 2009, 2010, 2011, 2015 and following sections herein). CTX images have shown, however, that THEMIS data alone cannot reliably be used to delineate all flow margins on a regional basis or to determine accurate flow dimensions, as CTX images show much more clearly whether margins are primary emplacement margins or are embayed (see Section 5.2). Mars Express HRSC images also provide complementary information at a similar scale, although are not used in the current study.

Analysis of CTX images allows mapping and characterization of volcanic features in the study area southwest of Arsia Mons. Within the extensive flow fields, CTX images reveal: i) small circular to elongate vents that commonly occur in clusters, ii) long, narrow channels, and iii) numerous prominent, elongate, sinuous lava flows, many of which can be traced for 100 + km. Two main types of elongate, sinuous lava flows are evident (Fig. 2A): 1) large, relatively thick, higher albedo (bright in CTX images) flows with rugged upper surfaces that display medial channel and levee systems and which may have broad, distal flow lobes, and 2) small, relatively thin, lower albedo (dark in CTX images) flow lobes with mostly featureless surfaces that are typically associated with narrow lava channels or lava tubes. In the south part of the study area and beyond, the flow morphology changes. Wider, larger, and in some cases less well-defined flow units are evident here (Fig. 2B); south of the study area these broad lobes appear to coalesce to form a vast volcanic plain (Crown and Berman, 2012; Crown et al., 2013; see also Giacomini et al., 2009, 2012). Along the southern margin of the Tharsis region, large, ridged, and sometimes platy, sheet flows along with a series of presumed volcanic plains embay the cratered highlands.

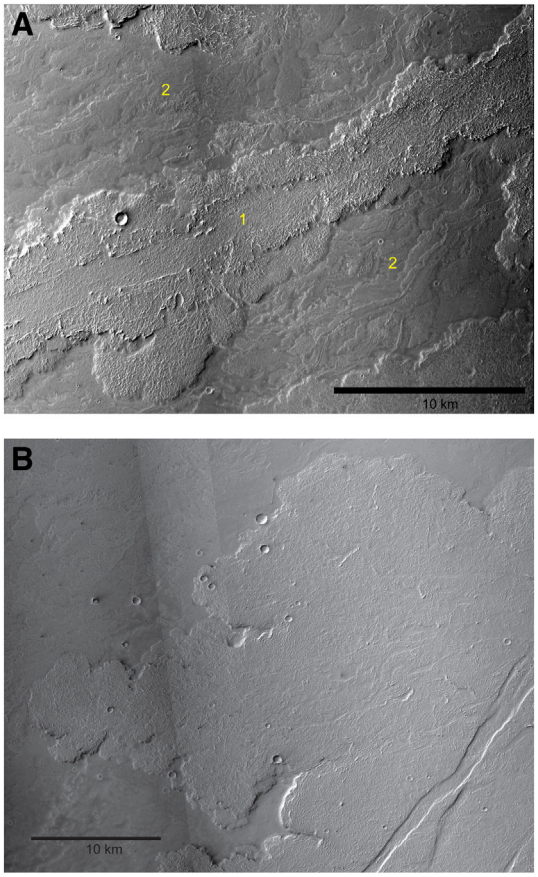

Fig. 2. A. CTX images (P04_002500_1563 and B02_010464_1545) showing the two main lava flow types recognized in the study area: 1) large, relatively thick, bright flows with rugged upper surfaces; and 2) small, relatively thin, dark flows with mostly featureless surfaces that are typically associated with narrow lava channels or lava tubes. Note the large central channel with a depressed surface in the rugged lobe (at center) as well as the complex lateral levee system. Illumination is from the northwest (upper left) in all CTX images shown in Figs. 2–6. B. CTX images (B12_014354_1531, B12_014143_1553, and P17_007748_1554) showing broad lobes that are progressively more prevalent in the southern portion of the flow field study area. Note that the flow margin sinuosity indicates broad lobes advanced as compound features consisting of sub-lobes of various sizes.

5.1.1. Bright, rugged flows

The distinctive bright, rugged flows southwest of Arsia Mons extend N/NE to S/SW and are concentrated in the upper central and eastern parts of the study area. Individual lava flow lobes exhibit exposed lengths of 100 km or more in the study area, which should be considered minimum values given the evidence of burial of rugged flows upflow to the north of the region of interest. The longest exposed flow length in the study area exceeds 250 km. Flow widths for bright, rugged lobes vary considerably along the flow length; flow widths are typically between 3 and 10 km but can approach 20 km in some locations. Bright, rugged flows display patterns of small high-standing bedrock exposures that indicate local flow direction and delineate central channels and flow levees (Fig. 3). Channels are typically bounded by a distinct, linear to curvilinear margin and display relatively constant widths (typically 1 to 3 km), although in some cases channel widths are observed to vary significantly downflow. The central channel surfaces are typically lower in elevation than the surrounding flow surface and may be covered by darker material. Major levee systems commonly make up much of the flow width and consist of coalesced lobes that have spread laterally from the edges of the central channel. These breakout lobes may extend to, and define, the outer flow margins. Some larger lobes appear to disrupt a pre-existing flow levee and form side lobes, such

Please cite this article as: Crown, D.A., Ramsey, M.S., Morphologic and thermophysical characteristics of lava flows southwest of Arsia Mons, Mars, J. Volcanol. Geotherm. Res. (2016), http://dx.doi.org/10.1016/j.jvolgeores.2016.07.008

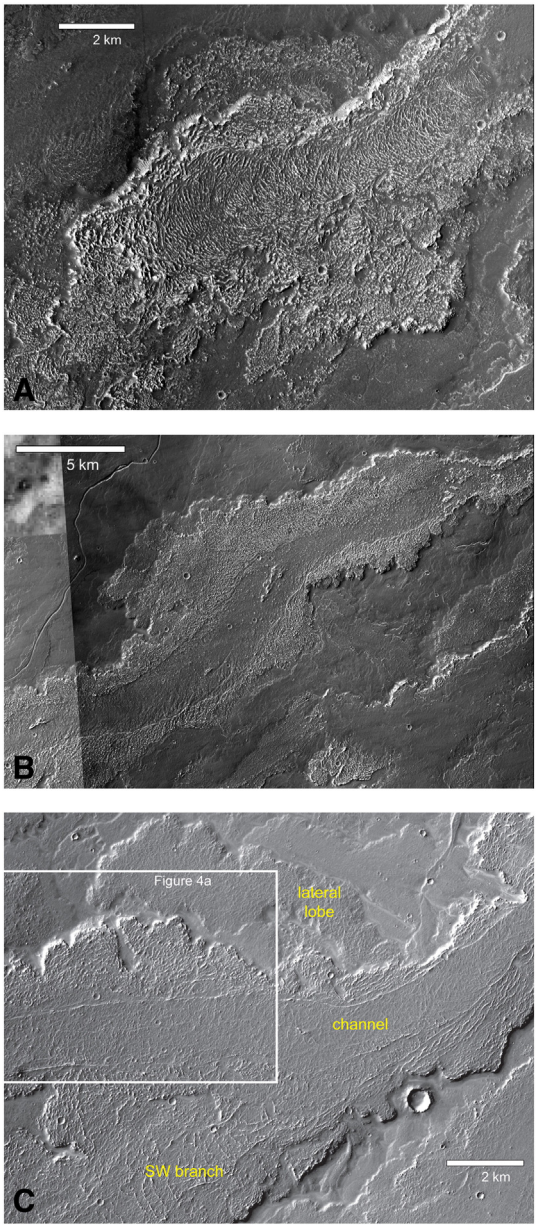

Fig. 3. A. CTX image (P16_007471_1586) showing a bright, rugged flow lobe with a ridged central channel and a levee system composed of small lateral breakout lobes. B. CTX images (P0_001590_1567 and P01_001524_1569) showing a rugged flow with a central channel and lateral levees. The widening of this flow (central part of the image) may indicate temporary flow front stagnation followed by renewed advance. C. CTX image (B02_010385_1569) showing a rugged flow with a central channel that exhibits a large branch extending to the southwest. Note also the large lobe extending from main flow to the northwest which could be a lateral lobe from the main channel or from an earlier flow. White box shows extent of Fig. 4a.

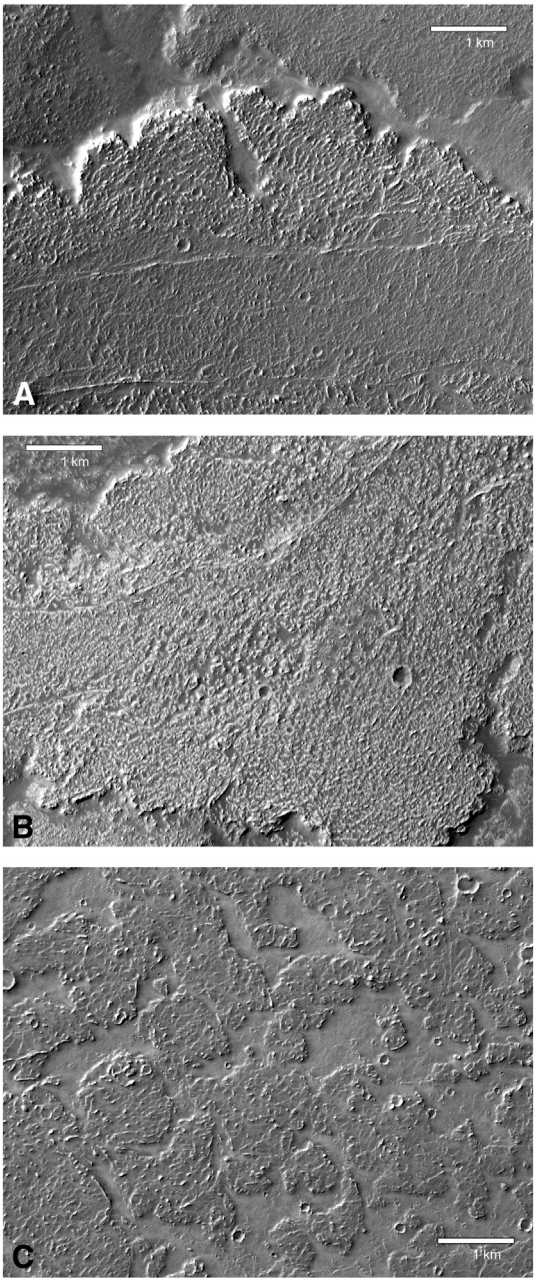

Fig. 4. A. CTX image (B02_010385_1569) showing an example of the ridged flow texture in the breakout lobes that form levees in a channelized, rugged lava flow. See Fig. 3C for location. B. CTX image (P16_007471_1586) showing the knobby flow texture on a central channel and the lateral levees in rugged lava flow. C. CTX image (B19_017097_1541) showing the platy flow texture in a broad flow lobe. Note the patches of flow surface with subdued ruggedness (i.e., plates) separated by low-lying smooth regions.

that the flow exhibits a branching morphology. The planform shapes and margins of the bright, rugged flows can be complex due to flow branching and complicated sequences of lateral spreading and breakout, suggesting complex spatial and temporal histories for individual flows. The flow cross-section at any given point, changes in flow cross-section downslope, and the overall flow shape record a delicate balance between supply history, advance of the flow front, and lateral spreading and levee development. The rugged flow surfaces display prominent ridged and/or knobby zones; in some cases, flow surfaces are less rugged and show platy morphologies (Fig. 4). Dark regions occurring in local, low-lying areas within higher-albedo rugged surfaces and as larger zones within central channels and extending across flow surfaces may be the result of mantling of the flow surface by fine-grained materials and/or surfaces of younger, dark, smooth lavas.

Examples of bright, rugged flows are shown in Fig. 3. Fig. 3A highlights a flow lobe with ridged texture forming the surface of its central channel. The flow margins appear to have been formed by small lateral breakout lobes that served as levees to retain lava in the main channel and foster advance at the front. In several places on the south side of the flow, ridge patterns indicate the flow direction for lava that disrupted the curvilinear margin of the central channel, and fed lateral breakouts. A rugged lava flow with an extensive central channel with a mostly dark, depressed surface is shown in Fig. 3B. Lateral levees consist of small breakout lobes extending from the central channel. The

Please cite this article as: Crown, D.A., Ramsey, M.S., Morphologic and thermophysical characteristics of lava flows southwest of Arsia Mons, Mars, J. Volcanol. Geotherm. Res. (2016), http://dx.doi.org/10.1016/j.jvolgeores.2016.07.008

flow widens considerably in the middle of the figure; this widened zone may have occurred due to temporary stagnation of the flow front (resulting from changes in local topography and/or lava supply) and then renewed advance. Fig. 3C displays a rugged flow with lateral levees formed by a series of breakout lobes and a large lateral branch that extends to the northwest, as well as a branch extending from its central channel to the southwest. The planform morphology of this flow illustrates the spatial and temporal complexities of emplacement processes for these rugged flows. Close-up views of the primary flow surface textures are shown in Fig. 4. Fig. 4A shows a channelized rugged flow with ridged texture dominating a series of lateral breakouts. Fig. 4B displays knobby texture characterizing both the central channel and levees of a rugged flow. A flow with platy texture, in which patches of the flow surface with moderate ruggedness are separated by low-lying smooth regions, is shown in Fig. 4C. Gradations between the ridged and knobby textures are commonly observed, and the degree to which the platy texture forms is observed to vary spatially.

5.1.2. Dark, smooth flows

Individual flow lobes are more difficult to fully discriminate in regions dominated by the dark, smooth flows, which are typically smaller than the rugged flows and whose margins exhibit less relief and are typically not as distinct (Fig. 5). However, CTX images do reveal both individual dark flows that may extend for distances

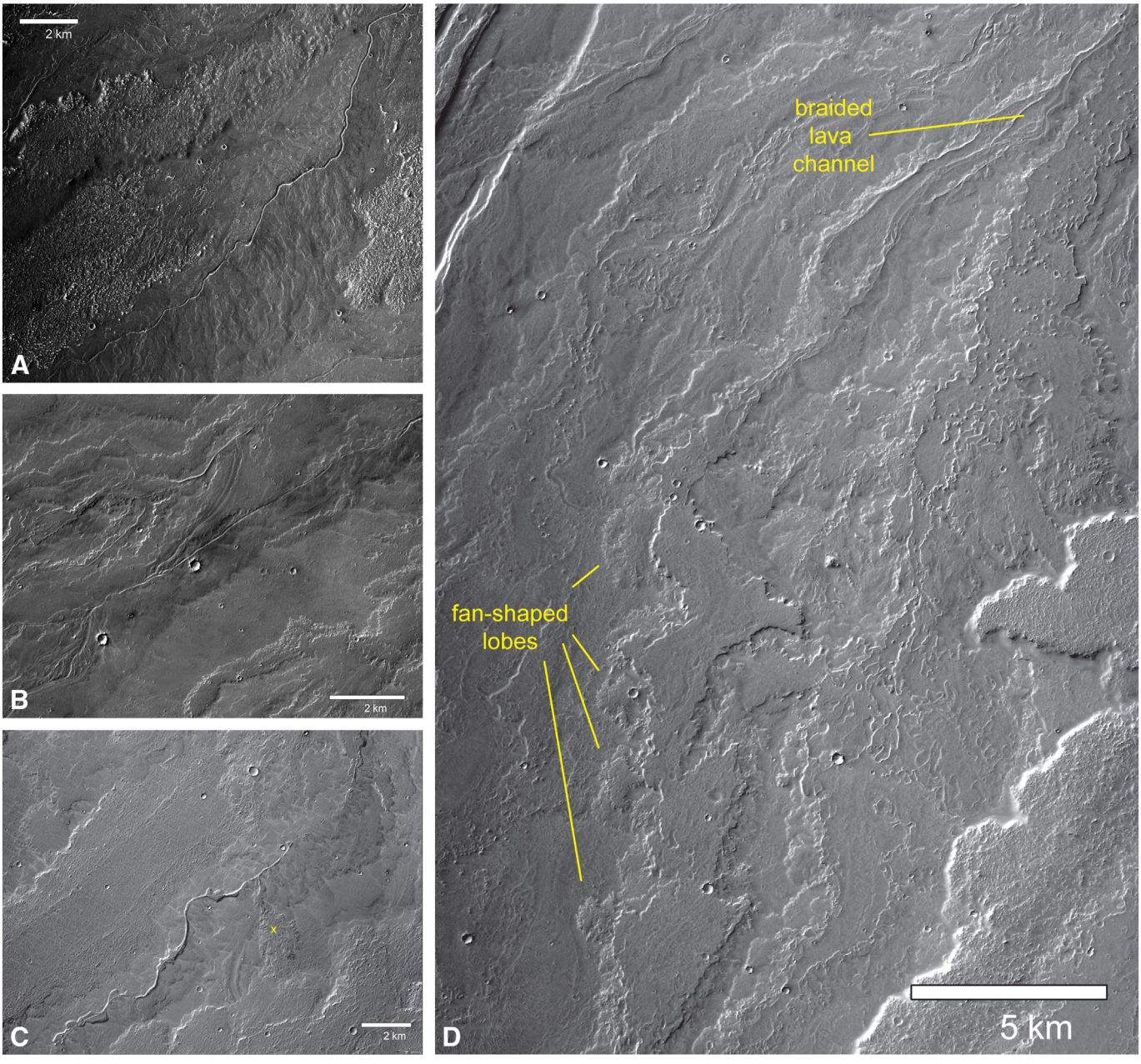

Fig. 5. A. CTX image (P04_002711_1560) of a continuous lava channel at the crest of a local topographic high whose flanks are composed of dark, smooth lava flow lobes. B. CTX image (G23_027171_1572) showing a discontinuous lava channel where small dark flows have accumulated; branching and braided channel morphologies are observed. Flow direction is from the northwest to the southeast. Note also the terraced, digitate margins of flows (at lower right) that may be due to flow inflation. C. CTX images (G22_026670_1581, P12_005889_1598, and B02_010385_1569) showing a discontinuous distributary system, associated dark flows, and steep-sided sinuous plateaus. Discontinuities in the distributary system may be due to the presence of roofed lava tube segments and/or partial burial of a channel system by overflowing lavas. Note that the dark lavas associated with the distributary system cover a channelized, rugged flow to the northwest, and the prominent breakout lobe (x) extending from the sinuous ridge at the crest of distributary system. Sinuous plateaus are interpreted to be inflation features that formed over a lava channel/tube system. D. CTX image (P15_006891_1535) showing a braided lava channel (at upper right) that continues into a series of steep-sided sinuous plateaus. The plateaus have small, digitate, fan-shaped lobes of dark lava emanating from their margins, particularly to the west.

Please cite this article as: Crown, D.A., Ramsey, M.S., Morphologic and thermophysical characteristics of lava flows southwest of Arsia Mons, Mars, J. Volcanol. Geotherm. Res. (2016), http://dx.doi.org/10.1016/j.jvolgeores.2016.07.008

comparable to the commonly larger rugged lobes, as well as assemblages of numerous smaller dark lobes. In some cases, long narrow channels occur on local topographic highs with dark flows spreading laterally from the central raised zone. Some narrow channels are continuous for long distances and others occur as discontinuous segments along a sinuous trend. These features are likely to be distributary systems that consist of a combination of segments of open channel, roofed lava tubes, and collapsed lava tubes. Some discontinuities in channels may be due to infilling by later flows emanating from the channel system due to blockages downstream and/or an increase in supply. Crown (2016; see also Crown et al., 2015) mapped 219 channels and channel segments within dark, smooth flow units in the study area, nearly 80% of which were between 5 and 40 km long. These volcanic channels commonly exhibit relatively uniform widths and also show branching and braided morphologies. In some cases, sinuous ridges and plateaus are observed along the trend of a lava channel/tube system (Fig. 5C,D). These typically have smooth upper surfaces and steep margins; locally, small, highly digitate, fan-shaped lobes appear to emanate from some sinuous plateau margins. We interpret these sinuous ridges and plateaus as inflation features that formed by excess lava flowing through a channel/tube system. Bleacher et al. (this volume) describe similar sinuous ridges and plateaus within Pavonis Mons lava flow fields on flows that extend from the SW rift apron into the plains to the east. Lava rise ridges, defined as elongate inflation features with length/width rations >10, have been described for a series of lava flows in Queensland, Australia. These features are prominent local topographic highs that form ridges or plateaus up to several hundred meters wide and extend for tens of kilometers (Stephenson et al., 1998; Whitehead and Stephenson, 1998). The digitate, fan-shaped lobes may be analogous to small pahoehoe lobes that extend from lava tubes, channels, and inflation features (including sinuous tumuli) in basaltic lava flow fields on the Earth (e.g., Orr et al., 2015).

Examples of dark, smooth flows and associated lava channels/tubes and other volcanic features are included in Fig. 5. Fig. 5A shows a continuous lava channel at the crest of a curvilinear topographic high. Small dark lobes extend laterally from the channel and dominate the flanks of this distributary system. The sinuous channel has a relatively constant width and dark flows associated with this channel embay and extend across the surfaces of adjacent rugged flows. Bleacher et al. (2007b) observed lava flows with similar morphologies (sinuous to linear ridges exhibiting sinuous chains of collapse pits or elongate depressions along the ridge crest) on the flanks of Olympus Mons and characterized them as tube-fed flows. A lava channel in a region dominated by dark, smooth lava flows is shown in Fig. 5B. The channel is discontinuous and poorly defined in a zone where small flows appear to have accumulated adjacent to the channel (upper right in Fig. 5B). To the southwest, the channel branches into two main segments, one of which shows a braided morphology. Flows to the southeast in Fig. 5B (bottom right) exhibit terraced margins that are highly sinuous at a small scale; these characteristics suggest flow inflation (e.g., Garry et al., 2012). Fig. 5C displays a discontinuous distributary system and associated dark, smooth flows. The trend of the distributary system is defined by a combination of elongate depressions, a sinuous ridge, and a series of steep-sided sinuous plateaus that straddle the sinuous ridge. Discontinuities may be due to partial burial of segments of an open lava channel and/or transport of the lava in a roofed lava tube. The sinuous ridge and plateaus are interpreted to be inflation features formed over a lava channel/tube system due to local increases in lava supply that were insufficient to cause emplacement of lateral breakout lobes. Collectively these features may be a type of elongate lava rise (after Walker, 1991; see also Stephenson et al., 1998; Whitehead and Stephenson, 1998). From one locality along the sinuous ridge, a lava flow lobe extends to the south and appears to be a breakout from the main distributary system. A lava channel with braided morphology that continues into a series of steep-sided sinuous plateaus is shown in Fig. 5D. The plateaus have small, digitate, fan-shaped lobes of dark lava emanating from their margins, particularly on the western side. The occurrence and morphologic characteristics of the sinuous plateaus indicate accumulation of lava along a lava channel/tube system, inflation of those lavas, and subsequent breakouts from the margins of the inflated features.

5.2. Flow interactions and flow field stratigraphy

CTX images reveal flow patterns and local interfingering and overlapping relationships in the study area that allow reconstruction of the complex flow field surfaces. Distinct embayment relationships are observed between and among the different flow types (Fig. 6). Darker channel-/tube-fed flows are commonly younger than the adjacent thicker, bright, rugged flows; however, this is not always the case. The observed diversity and complexity of interactions between flows may suggest that lava sources with different eruptive styles and magnitudes were active contemporaneously. Further to the south in the study area and beyond to the southwest, broad flow lobes (Fig. 2B) are partially buried by both types of elongate lobes. The earlier work of Bleacher et al. (2007a) using HRSC images showed consistent embayment of tube-fed flows by channel-fed flows on the main flanks of Arsia Mons but less consistent relationships in the plains to the south, where our current observations are concentrated.

Superposition relationships and surface morphologies within the Arsia Mons study area suggest complex interactions between flows (Fig. 6); for example, burial of one flow by another and sharp and gradational contacts between adjacent flows are apparent. The prominent and distinct margins of the bright, rugged flows are key indicators of flow lobe superposition, with loss of sinuosity and small-scale breakouts at their embayed margins. The darker flows are commonly observed to be deflected by the thicker margins of the bright, rugged flows, but in some areas dark flows are observed extending onto and partially to completely burying the rugged levees and surfaces of bright flows. In some areas, the dark flows appear to inundate rugged flow surfaces but the larger topographic elements of the underlying rugged flow surface (e.g., flow ridges and impact craters) are preserved. Darker flows are also seen to inundate and be topographically controlled by the central channels within bright flows. In several locations, lateral breakout lobes from the bright, rugged flows are observed to cover darker flow surfaces and the narrow channels associated with the darker flows. Contact relationships between flows of similar brightness are also observed, although it can be difficult to confidently interpret relative ages in some of these cases.

Specific examples of local stratigraphic relationships and interactions between lava flows in the Arsia Mons flow field study area are included in Fig. 6. Superposition of rugged flow lobes is shown in Fig. 6A. The subdued ruggedness and platy nature of the lowermost flow is consistent with its older relative age which is clearly indicated by superposition. Dark, smooth flows embay both rugged flows in this example and clearly utilized low-lying regions in the rugged flow surfaces to advance. Fig. 6B shows an example in which a bright, rugged lobe is the youngest flow in the local setting. This is indicated by small lobes that define the outer edge of the lateral levee system clearly burying parts of the narrow channel associated with the dark flows. Fig. 6C shows different styles and degrees of embayment of a bright, rugged flow by dark, smooth flows. The northern margin of the rugged flow is completely buried by the dark flows. The dark flow surfaces to the northeast are smooth and only extend short distances across the surface of the rugged flow, with one small lobe reaching the central channel. To the southwest, the same dark flows appear to have extended much of the way across the rugged flow surface. Here, the irregular surface texture is attributed to incomplete burial of the rugged flow surface and perhaps local inflation within the dark flows as they advanced through the rugged topography of the older flow surface. Incomplete burial of that surface is indicated by larger topographic elements "showing through" the dark flows in small patches as kipuka of the lower flow. It is likely that

Please cite this article as: Crown, D.A., Ramsey, M.S., Morphologic and thermophysical characteristics of lava flows southwest of Arsia Mons, Mars, J. Volcanol. Geotherm. Res. (2016), http://dx.doi.org/10.1016/j.jvolgeores.2016.07.008

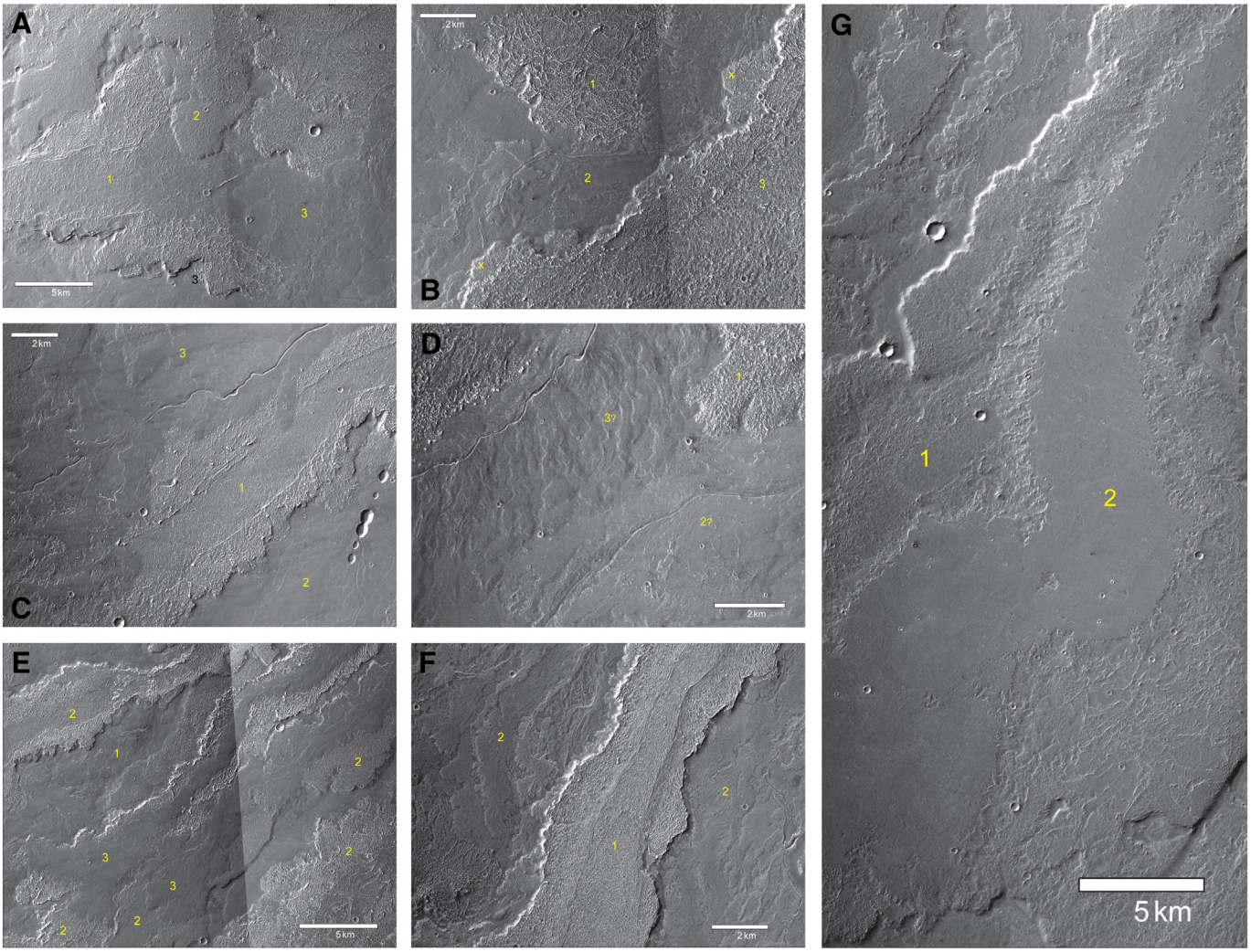

Fig. 6. Examples (6A–G) of the stratigraphic relationships and interactions between lava flows in the Arsia Mons flow field. CTX images reveal embayment relationships between and among the different flow types recognized. In Fig. 6A–E, local stratigraphic relationships between and among flows are shown (1 = oldest, 3 = youngest). Fig. 6A shows CTX images (B02_010464_1545 and P04_002500_1563) of a bright, rugged flow extending from the north covering a rugged flow with platy texture that extends across figure from east to west. Both rugged flows are embayed by dark flows from the east. B. CTX images (P04_002500_1563 and P05_002856_1568) showing a bright, rugged flow with a central channel and lateral levees (extending from northeast to southwest) that covers dark flows (at center), which in turn partially bury a rugged flow with a platy surface (extending to south from the top of figure). Note that in several locations (x) small lobes that define the northwestern edge of the lateral levee system bury a narrow channel associated with the dark flows. C. CTX image (P01_001590_1567) showing dark flows associated with a narrow channel (top) embaying a bright, rugged flow. Note the pit chain, narrow channel, and associated dark flows to the southeast that also appear to embay the rugged flow. The dark flows have completely buried the northern margin of the rugged flow and extend across its surface. At the bottom left, the irregular surface texture is due to incomplete burial of a rugged flow by the dark flows and perhaps local inflation of the dark flows as they advanced through the rugged topography of the flow surface. D. CTX image (P04_002711_1560) showing dark flows from two narrow channels embaying a rugged flow (at upper right) and interacting with each other. It is not clear which set of dark flows is younger. Numerous small lobes extending from the northern channel (see also Fig. 5A) can be identified based on the presence of distinct flow margins that give the appearance they are younger; however, the dark flows associated with the southern channel may have flowed up against and into gaps between these lobes. Inflation of the southern dark flows may also have helped to obscure the relative flow stratigraphy along this contact. E. CTX images (P01_001524_1569 and P04_002500_1563) showing a series of bright rugged flows extending from northeast to southwest. The northernmost flow displays a well-developed central channel and lobate lateral levees. At center, dark flows appear to have been captured within the local depressions defined by the central channels of two rugged lobes. These dark flows extend downslope and laterally across the rugged pre-existing, rugged surfaces to various distances. F. CTX image (P16_007471_1586) showing a bright, rugged flow that is embayed by dark flows on both sides. Comparison of the margins of the rugged flow shows differences in sinuosity due to the presence of a set of small lobes to the west that represent the outer edge of the lateral levee system. The difference in sinuosity could be due to formation of these outer lobes along only one flow margin or a different degree of embayment on the different sides of the flow, perhaps coupled with larger scale flow inflation to the east. G. CTX image (P18_008038_1544) showing a rugged flow with platy surface texture whose center contains a smooth plateau rising above the rugged flow surface. The smooth plateau has steep, jagged margins and a sinuous planform that suggests it may represent the location of the central channel of the rugged flow. The smooth plateau may have formed by dark lavas that were captured by the central channel of the rugged flow and then inflated in a fairly uniform manner above the flow surface.

some of the impact craters observed on the dark flows are incompletely buried craters that formed on the rugged flow surface below. Dark flows advancing across the ridged, knobby, and cratered surfaces of rugged flows could be deflected by the rugged topography and also cause flow stagnation. Therefore, any resulting inflation might show patterns that mimic the texture of the underlying rugged flow surface, and where inflation progressed, it could have resulted in inverted local topography relative to the original flow surface (i.e., inflation may have been concentrated in what were local topographic lows on the underlying rugged flow surface). The occurrence of the irregular surface texture on otherwise dark, smooth flows in similar localities across the study region can be considered representative of flow superposition of rugged flows by dark (and less viscous) flows. The presence of mixed patches of dark and bright flow surfaces and observations of steep margins, jagged edges, and through-going patterns likely indicates inflation of dark flows that overlie rugged surfaces.

Please cite this article as: Crown, D.A., Ramsey, M.S., Morphologic and thermophysical characteristics of lava flows southwest of Arsia Mons, Mars, J. Volcanol. Geotherm. Res. (2016), http://dx.doi.org/10.1016/j.jvolgeores.2016.07.008

The contact zone between dark flows associated with two nearby narrow channels is displayed in Fig. 6D. The northern channel appears to have laterally fed numerous small lobes that extended to the south. These lobes exhibit local variations in relief that delineate at least parts of their margins. The southern channel is surrounded by dark flows that cannot clearly be divided into discrete lobes, and the contact relationship between the two sets of dark flows is unclear. The better delineation of flows from the north and possible deflection of several lobes suggests that they may be younger; however, the southern flows may have flowed up against and into gaps between these lobes and perhaps also inflated against the topographic barrier of the northern flows, suggesting that they could be younger.

Capture of dark, smooth flows in pre-existing central channels of two rugged lobes is shown in Fig. 6E. In both cases, the dark flows cover the central channelized regions of the rugged flows, extend downslope over them, and then spread to inundate the rugged flow surface farther downslope. This creates a hybrid morphology in which the flow margin is the steep-sided levee of a bright, rugged flow and the surface is dark, smooth lava. This type of relationship between the dark and bright flows also suggests a lower viscosity for the dark flows, and directly indicates the age relationship between these flow types in this location.

Fig. 6F displays a bright, rugged lobe surrounded by dark lava flows. The east and west sides of the rugged flow exhibit differences in sinuosity. The western side displays a higher sinuosity due to the presence of a set of small lobes that represent the outer edge of the lateral levee system. These may represent the original flow margin that formed when the flow front passed this location or they may have formed as breakouts from the levees. The eastern side does not exhibit these small lobes. This asymmetry can be attributed to differences in flow emplacement, embayment, or relative age. Perhaps the small, outer lobes did not form on the east side of the flow, and asymmetric levee development could be related to differences in the local topography (i.e., slope) and roughness of the pre-flow surface. Alternatively, the margin of the rugged flow could be partially buried to the east; a larger degree of embayment could bury or obscure any small breakout lobes that formed there. If dark flows from the east banked up against the rugged flow, they may also have inflated, further hindering identification of small lateral breakout lobes. CTX images have been used to interpret relative ages of the flows and suggest that the bright rugged flow is older than the dark, smooth flows to the east and west. This is based on observations of dark, smooth flows following and flowing into indentations along rugged flow margins and extending onto them, as well as a lack of clear superposition of small lateral lobes on top of dark, smooth lava to the west. Because the relative ages between the flows can be difficult to interpret, an alternative scenario might be that the small, breakout lobes from the levees are younger than dark, smooth flows to the west. This example shown in Fig. 6F demonstrates that detailed analysis of flow margins using high-resolution images is essential for accurate studies of flow emplacement, as flow widths and flow margin characteristics are key quantitative input parameters for models that estimate flow properties (e.g., Hulme, 1974; Fink and Zimbelman, 1990; Lopes and Kilburn, 1990; Bruno et al., 1994; Rowland et al., 2004; Glaze et al., 2009). Many past studies that calculate properties such as flow viscosity have assumed that the entire flow width has been observed/measured. It is clear from the Arsia Mons flow field that this is probably not the case. Fig. 6G shows a rugged flow with a central smooth interior plateau with steep, jagged margins that likely corresponded to a central channel. We interpret its occurrence, shape, and surface characteristics to be due to capture of dark lava by the topography of the central channel of a rugged flow, subsequent flow down the channel, and later inflation to a level above the rugged flow surface. This example further illustrates the highly complicated nature of these flow field surfaces, but also that CTX images can be used to discriminate complex flow types and superposition relationships.

5.3. Thermophysical and spectral variability

5.3.1. Thermophysical diversity

The unusual thermal behavior south of Arsia Mons was initially noted by Bandfield (2009), who attributed highly variable slopes in TES and THEMIS apparent emissivity spectra to sub-pixel temperature mixing caused by rough surfaces with steep slopes. These topographic slopes caused by roughness elements (e.g., blocky lava flows) have variable surface temperatures due to shadowing, which results in multicomponent thermal mixing and the spectral distortions observed. Modeling of these spectra showed that RMS slopes of ~30° are needed to represent the spectral distortions (Bandfield, 2009). These surfaces therefore represent some of the roughest on the planet with centimeter to meter scale topographic elements. Depending on the size of the TIR pixel and degree of thermal mixing, surfaces with such a large fraction of topographic slopes and/or roughness elements result in thermally-emitted radiance with a high degree of anisothermality, especially at times of high solar incidence angles. This thermal mixing at the cm–m scale is quite different than the spectral mixing at the micron-scale noted by Ramsey and Fink (1999), which assumes an isothermal pixel and models higher percentages of micron-scale roughness (i.e., surface vesicularity) based upon an emissivity spectrum closer to that of a blackbody (e.g., emissivity equal to unity at all wavelengths). Anisothermality at the pixel scale regardless of the micron-scale roughness results in non-linear mixing in radiance space as opposed to linear mixing in emissivity space. The distinct spectral slopes in the derived apparent emissivity spectra arise depending on the value chosen for the maximum assumed emissivity or the presumption of a uniform surface temperature within the field of view. It was this analysis of the TES and THEMIS spectral slopes that allowed Bandfield (2009) to model and describe the range of surface roughness based on a Gaussian distribution of random slope azimuths.

Southern Tharsis is generally considered to be spectrally bland in the IR due to the assumption of significant amounts of surface dust present throughout the region. Here, dust produces a relatively high visible albedo (range ~0.23–0.25) and moderate dust cover index values (DCI, range from ~0.93 to 0.98) (e.g., Ruff and Christensen, 2002). Ramsey and Crown (2010) analyzed day and night THEMIS IR images of this region, confirmed the rough surfaces modeled by Bandfield (2009), and also observed unusual lava flow scale thermophysical variability. The DCI range reveals that there are some areas relatively free of dust at the spatial resolution of TES (3 km/pixel). At the spatial resolution of THEMIS (100 m/pixel), many of these regions can be associated with individual flow units. Based on the results of Bandfield (2009) and examination of shadowing in high-resolution images, the rugged, higher-albedo flows have centimeter- to meter-scale roughness with some areas being partially infilled by aeolian material. Rocky surfaces on Mars that are relatively free of dust typically show warmer nighttime temperatures and cooler daytime temperatures, with the opposite behavior for surfaces that are either uniformly fine-grained or for rocky material that is heavily mantled by fine-grained dust. Fig. 1C shows that flow surfaces southwest of Arsia Mons exhibit all styles of thermophysical behavior indicating either a) non-uniform mantling of dust and therefore a mixing of temperature and albedo effects at the sub-pixel scale, b) the presence of different aged flows with the younger flows being less dust covered, and/or c) the preferential removal and/or trapping of dust on certain flows. Furthermore, flow surfaces are also found in the same vicinity that exhibit no apparent change in their diurnal temperature, with some surfaces remaining uniformly cool and others uniformly warm throughout the diurnal cycle. For this level of thermophysical variability to be present in a relatively small region is unusual on Mars. If the lava flows southwest of Arsia Mons have been uniformly mantled by airfall dust at a constant rate since their emplacement, the thermophysical response would identical to other dusty regions on Mars (i.e., surfaces with uniformly low thermal inertia and hence, warmer temperatures in the day and correspondingly cooler surfaces at night). On the other hand, if the lava flows were of significantly different ages, the younger flows should

Please cite this article as: Crown, D.A., Ramsey, M.S., Morphologic and thermophysical characteristics of lava flows southwest of Arsia Mons, Mars, J. Volcanol. Geotherm. Res. (2016), http://dx.doi.org/10.1016/j.jvolgeores.2016.07.008

have less dust cover and behave thermally as rocky surfaces (i.e., surfaces with higher thermal inertia and hence, cooler temperatures in the day and correspondingly warmer surfaces at night). We see both of these end-member cases (a and b above) in the southwest Arsia Mons flow field. However, neither would explain flows that show no temperature change throughout the Mars day. The most likely cause of this unusual behavior is that the rugged, blocky flows have surfaces that consist of a combination of relatively low-albedo rocky surfaces, partially-mantled dusty (high-albedo) surfaces, and infilling of topographic lows by sand-sized particles (intermediate to lower albedo). Such a complex sub-pixel mixing scenario could result in a unique situation of relative thermal stability throughout the diurnal cycle. Regardless of the cause, these flows are of interest as their age and or roughness/topography have resulted in this state of unusual thermophysical behavior partially due to aeolian mantling and infilling.

5.3.2. High-resolution image comparisons

As described above, CTX images reveal the visible nature and diversity of the surfaces of lava flows southwest of Arsia Mons. The two primary flow types identified, a dominantly-smooth and possibly inflated (dark) flow type and a rough-surfaced (bright) flow type were further investigated by comparing HiRISE images to THEMIS spectral data. CTX images provide spatial context at the flow scale, whereas HiRISE images allow small details of the lava flow surfaces as well as aeolian modification to be resolved. We focused primarily on the brighter flow type in this analysis as those flows generally display the largest diversity of thermophysical behavior and spectral and thermophysical variations between lateral levees and central channel, and they clearly showed the presence of the aeolian infill material.

HiRISE images of the rugged flows reveal clusters of small rocky outcrops with albedo higher than the aeolian infill in the low-lying regions surrounding them (Fig. 7). For select locations, we ran unsupervised classifications to estimate a simple first-order surface coverage of lava outcrop versus fines (Crown et al., 2009). Typically, the intermediate- to lower-albedo, sandy infill covers 50–60% of the flow surface, and therefore would contribute this amount of spectral signal linearly to any averaged IR spectrum of a THEMIS pixel (e.g., Ramsey and Christensen, 1998). The remaining percentage of non-mantled flow surface would easily be enough to produce the scales of roughness documented by Bandfield (2009). The infilling material is distinctly different in albedo and spatial patterns than air fall dust. Dust would be expected to cover all surfaces (rocky and sandy) in the region equally, with perhaps some preferential removal by wind on the higher surfaces. In addition, small patches of transverse aeolian ridges (TARs) are frequently observed in the topographic lows, interpreted to be lithified relicts of prior, more pervasive aeolian activity. The dark aeolian material fills low-lying areas on the flow surface to a similar depth, above which the flow surfaces appear to be free of this material. The rocky outcrops on these rugged surfaces also reveal flow patterns, such as flow-perpendicular folding, that are most obvious in the rugged levees and at flow margins where the aeolian infilling material is not as pervasive (Fig. 7). HiRISE images demonstrate that flow surfaces still include a significant component of massive bedrock outcrops, which remain despite prolonged degradation by aeolian processes.

5.3.3. IR spectral diversity and flow morphology

THEMIS IR image data for the study area were obtained from the PDS archive maintained by the THEMIS science team. These data were preprocessed and downloaded using the THMPROC tool (http://www.thmproc.mars.asu.edu). The pixel-integrated brightness temperature and emissivity were extracted from these radiance data following atmospheric correction, as described in Section 4 (Fig. 8A). THEMIS spectral data were examined for defined regions of interest (ROIs) that were chosen based on high-resolution image analysis. These data were compared across the two dominant flow types as well as for variations both downflow and across individual flow units.

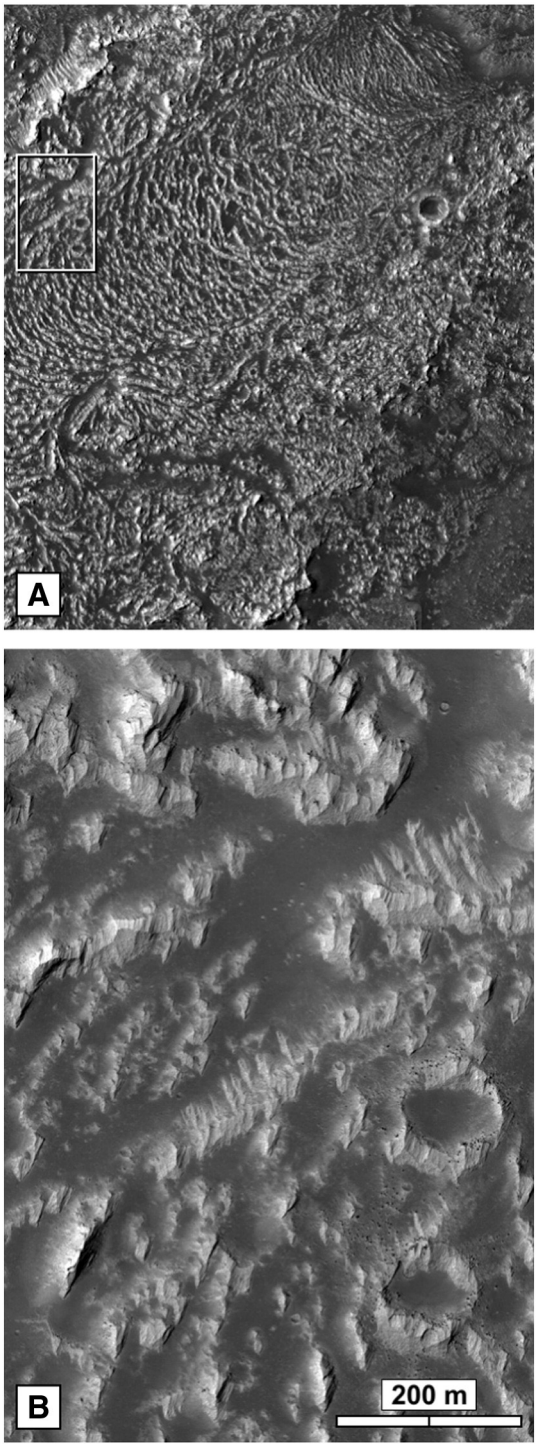

Fig. 7. HiRISE image (PSP_006614_1580) of a representative bright, rugged flow in the southwest Arsia Mons region. (A) Central channel and levee structure of the flow. The white box indicates the area shown in (B). An example of TARs is seen directly above the white box near the upper left corner of the image. (B) Detail of the lower-albedo aeolian infill material with outcrops of the topographically-higher, brighter lava flow surface visible.

Single regions of interest (ROI) averaging 16 THEMIS IR pixels were extracted from the atmospherically-corrected emissivity data (Fig. 8B,C). Spectra from these regions are shown in Fig. 9A. The IR spectra from the two flow types are statistically different, although their spectral shapes are similar both to one another and to basaltic spectra derived elsewhere on the planet (Bandfield, 2002). What is apparent in the spectrum of the bright flow (ROI #18) is the negative slope from

Please cite this article as: Crown, D.A., Ramsey, M.S., Morphologic and thermophysical characteristics of lava flows southwest of Arsia Mons, Mars, J. Volcanol. Geotherm. Res. (2016), http://dx.doi.org/10.1016/j.jvolgeores.2016.07.008

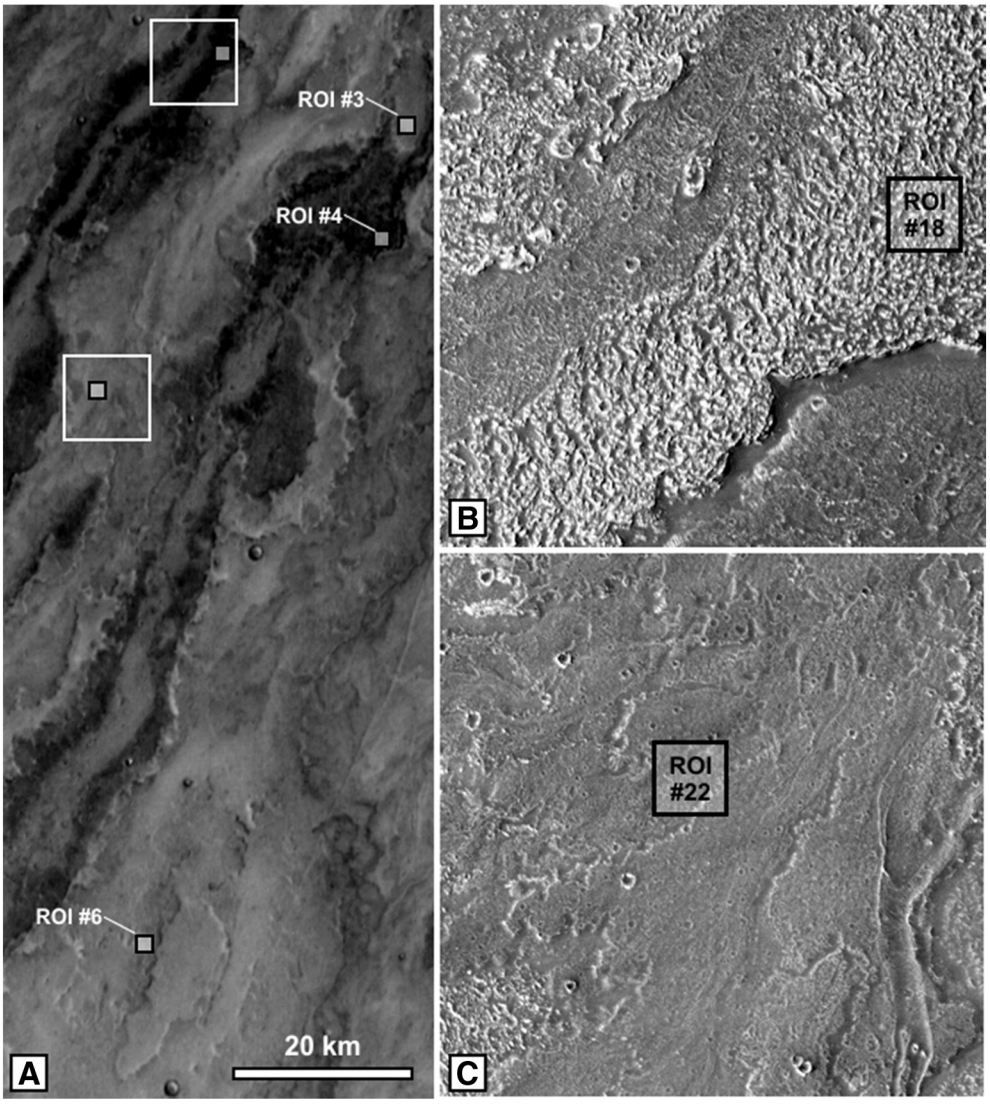

Fig. 8. THEMIS IR spectral regions analyzed in this work. (A) THEMIS daytime brightness temperature image following atmospheric correction and temperature/emissivity separation (THEMIS image I07370003). The white boxes indicate the regions shown in (B) and (C), with the smaller black boxes showing the regions of interest (ROIs) from which spectral data were extracted. ROIs #4 and #18 are from the bright, rugged flow type, and ROIs #3, #6, and #22 are from dark, smooth flow surfaces. (B) Part of CTX image (P05_002856_1568) showing the area of upper white box in (A) that includes part of a bright, rugged flow. The area of ROI #18 is noted. (C) Part of the same CTX image showing area of lower white box in (A) which is dominated by dark, smooth flows. The area of ROI #22 is shown.

~7.5 to 11.5 μm, which is significantly different than the slope in this region in the spectrum of the dark flow (ROI #22). This is commonly seen in pixels covering surfaces with two or more surface temperatures averaged together (e.g., Rose et al., 2014) and further supports the results of Bandfield (2009). A simple fit to the mixed spectrum using a negative linear slope line can serve as a proxy to remove/reduce this effect in order to accurately compare spectra from the different flow types. Upon correction the main absorption feature in the spectrum of the bright, rugged flow (ROI #18, corrected) remains significantly deeper than that of the dark, smooth flow, indicating that the bright, rugged flows are likely less dust covered. This also reinforces the thermophysical results for these flows, which indicate the bright, rugged flows are rockier with a corresponding diurnal temperature variation that is cooler in the day and warmer at night compared to other flows in the region. The rugged levees commonly have daytime temperatures ~4° lower than the warmer channels and the surrounding dark flows, indicating a slightly higher thermal inertia.

Emissivity spectra were also extracted in 24 other locations in the flow field, focusing on areas of different morphology (e.g., central channels vs. levees), traverses across and along individual flows, and additional sampling of the different flow types. ROI locations were also chosen based on spectral differences seen as color variations in standard decorrelation stretch (DCS) band combinations (Fig. 10). Color variations in a DCS of a thermal infrared radiance image typically indicate differences in composition, whereas variations in the intensity of a given color indicate temperature differences (Gillespie, 1992). Some of the color variations (especially those that are not correlated with surface features) are likely due to atmospheric and/or instrument variability. However, color differences related to specific flow units are evident and are confirmed by examining emissivity spectra (Fig. 9).

The locations of three representative ROIs are shown on Fig. 8A (#3, #4, and #6). The spectra from these locations (Fig. 9B) are similar to those in Fig. 9A, with the largest difference occurring once again between the rough flow levees of a bright, rugged flow (ROI #4) and dark, smooth flow surfaces (ROIs #3 and #6). The smooth flows have 9.3 μm absorptions that are 10–30% shallower than the rugged flow levees. The variation in spectral depth is likely due to the presence of dust mantling, whereas the overall shape is a function of the lava composition. ROI #6 has the shallowest spectral feature; it occurs on a flow that may be older than the flow from which ROI #3 was extracted.

Please cite this article as: Crown, D.A., Ramsey, M.S., Morphologic and thermophysical characteristics of lava flows southwest of Arsia Mons, Mars, J. Volcanol. Geotherm. Res. (2016), http://dx.doi.org/10.1016/j.jvolgeores.2016.07.008

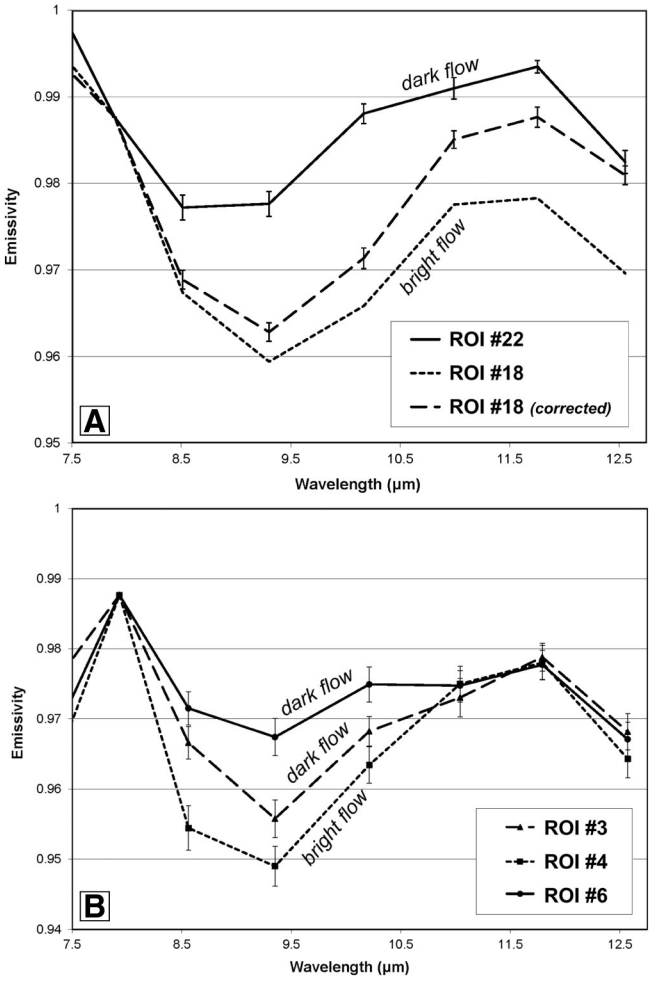

Fig. 9. THEMIS IR spectra extracted from processed I07370003 image. (A) Comparison of average spectra of ROI #22 (dark, smooth flow) and ROI #18 (bright, rugged flow), chosen to display the spectral diversity in the flow field. Spectra have the same general shape and indicate a likely basaltic composition. ROI #22, however, has a slightly deeper absorption at 8.5 μm that could be the result of a compositional variation of the lava or the presence of more dust on the surface of these flows. The higher overall emissivity also indicates the presence of more dust. ROI #18 shows a distinct slope from 7.5 to 11.5 μm that is commonly seen in anisothermal surfaces (e.g., Rose et al., 2014). Removal of that slope (ROI #18 – corrected) results in a spectrum that is still significantly lower in emissivity and statistically separable from the spectrum of ROI #22. This indicates that air fall dust mantling is not uniform across the flow field and that the rougher flows may in fact be less dusty. (B) IR emissivity spectra extracted from ROI's #3, #4, and #6 also show variability between flow units. The surface of the bright, rugged flow with the cooler daytime signature has the deepest spectral feature (ROI #4). See Fig. 8 for ROI locations.

That flow occupies the central channel of the bright, rugged (low daytime temperature) flow from which ROI #4 was acquired. Spectral variations between the smooth, darker flow units are likely due to the accumulation of dust and may reflect relative flow ages and/or the ability to retain dust once deposited on those surfaces. The spectrum of ROI #4 has the deepest spectral feature observed and was extracted from a flow levee that displays one of the strongest diurnal temperature variations in the region (Fig. 9B). This spectrum also has a slightly deeper absorption at 8.5 μm, which could indicate a different flow composition compared to the smoother flows. Alternatively, its spectrum may reflect a mixture of the lava flow composition plus the aeolian infilling material. The higher-albedo, rockier flows appear to have less pervasive dust mantling, however have more aeolian infilling of the low lying parts of the flows. In such cases, these flows are a checkerboard linear mixture of rock plus sand and present a target from which the actual lava composition can be extracted spectrally.

6. Discussion

As presented above, this investigation of the lava flow fields southwest of Arsia Mons and in northeast Daedalia Planum using imaging and thermophysical datasets has provided new characterizations of a) lava flow surfaces, including the effects of aeolian infilling and mantling; b) lava flow morphology and related emplacement styles; and c) the development of Martian lava flow fields, given the overlapping and interfingering relationships documented between adjacent flow lobes. Below we discuss further the volcanological implications of certain aspects of our results, including potential sources for the lava flows analyzed, inferences regarding flow rheology and implications for lava flow emplacement styles (including the role of flow inflation), and analogies between Martian and terrestrial flow fields.

6.1. Source vents

Analyses of Viking Orbiter images showed vast flow fields south of Arsia Mons with flow patterns radiating from the Arsia Mons SW rift (Carr et al., 1977). This early study along with the lack of identified vents within the rift apron near Arsia Mons in more recent work (i.e., Bleacher et al., 2007a) suggest that the primary source for lavas that accumulated to form the voluminous flow fields was the SW rift. Buried flank vents could also have contributed but some morphologic indication of these would be expected given the high spatial resolution of recently acquired images. The detailed investigation of part of the flow field presented here did not reveal flank vents within the study area. Results show long, rugged flows extending into the study area from the north but also that these flows cannot be easily traced northward to any obvious sources due to the overlapping nature of lobes within the flow field. In addition, the flow field appears to include extensive distributary systems that emplace smaller lobes of the dark, smooth lava type. With additional mapping of the flow field north of the study area, these distributary systems may be traced northward toward the SW rift, providing an indication of their full lengths and an assessment of the overall distributary pattern or patterns southwest of Arsia Mons. The narrow distributary systems and related dark, smooth flows are morphologically subtle relative to the rugged flows with prominent channels and levees but, from the research presented herein, these may have been of equal importance volumetrically in the overall emplacement of the flow field, or at least in the part of the flow field studied here. Knowledge of the history of magma production and related sequences of lava flow emplacement associated with the Arsia Mons SW rift are of fundamental importance in understanding the formation and evolution of the Tharsis volcanic province on Mars, given the volumes of lava involved and longevity of activity.

6.2. Flow rheology and emplacement style

Observations of and comparisons between the bright, rugged and dark, smooth flows provide insight into the relative rheologic properties of these flow types and their emplacement styles. In particular, surface roughness, flow thickness, branching behavior, and volcanological setting can be used to interpret relative lava viscosities and emplacement scenarios. The smoother upper surfaces, thinness, more numerous, and smaller lobes of the dark, smooth flow type suggest lower viscosity lavas than for the bright, rugged flows. TIR data show basaltic spectral signatures for both flow types; however, spectral variations do not clearly distinguish between potential compositional differences and differences caused by aeolian effects. Given the channel-/tube-fed nature of the dark flow type, the difference in viscosity may be the result of transport within an insulated distributary system that limits heat loss, rather than a significant compositional difference between the flow types. If the differences between the flow types are predominantly textural (rather than compositional), local supply (i.e., lava supply along an discrete path or to an individual flow lobe) may be a controlling factor

Please cite this article as: Crown, D.A., Ramsey, M.S., Morphologic and thermophysical characteristics of lava flows southwest of Arsia Mons, Mars, J. Volcanol. Geotherm. Res. (2016), http://dx.doi.org/10.1016/j.jvolgeores.2016.07.008

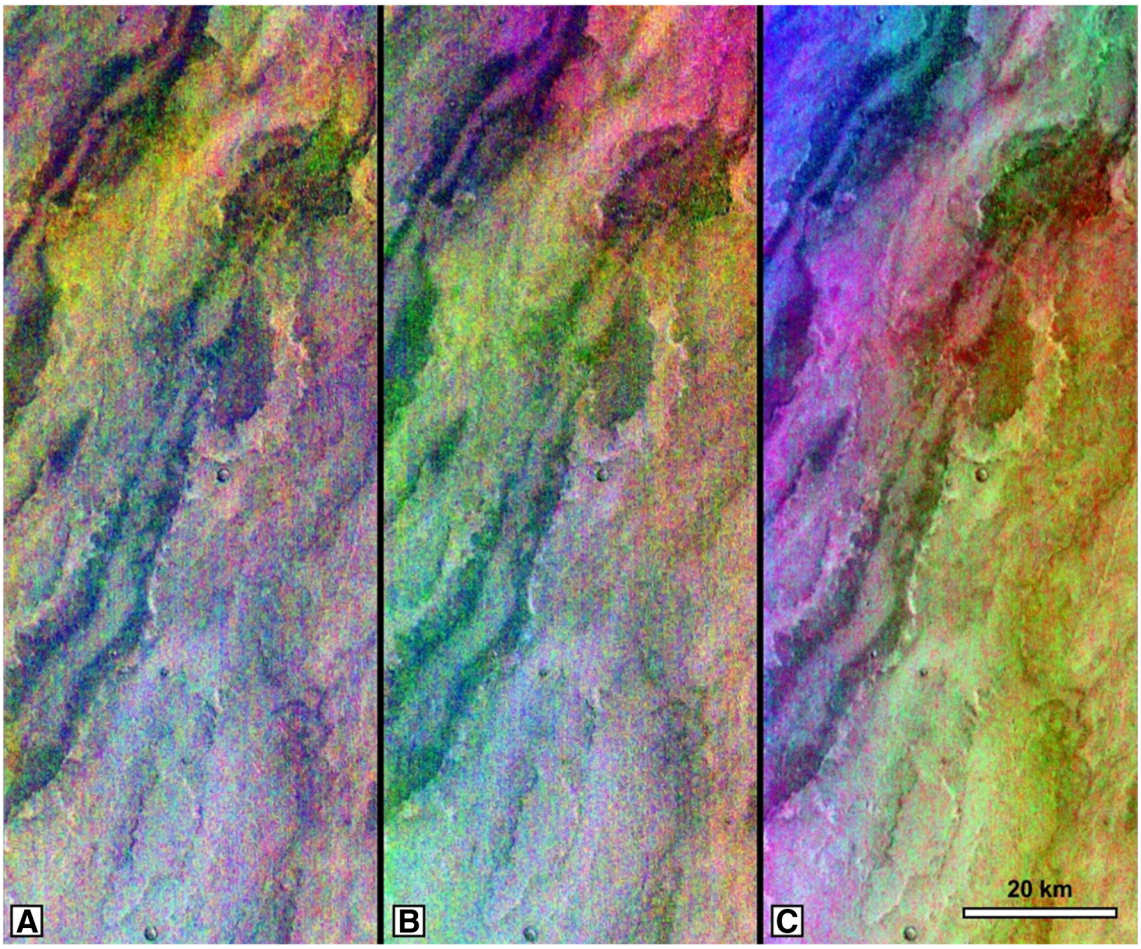

Fig. 10. Different decorrelation stretch (DCS) band combinations of the THEMIS IR radiance image (I07370003). The color variations are due both to atmospheric and instrument effects as well as correlated to individual flows and flow levees. (A) Bands 8, 7, 5 in R, G, B. (B) Bands 9, 6, 4 in R, G, B. (C) Bands 6, 4, 2 in R, G, B. See text for discussion.

(e.g., Rowland and Walker, 1990). For the SW Arsia Mons/NE Daedalia Planum region, we have not examined surface slopes for individual flow lobes but overall slopes for lava flows within the study region are consistently low (<2°). With local supply rates higher than some threshold value, larger, thicker, bright, rugged flows may have formed, whereas, below that threshold, lava would have been transported through the narrow tube and channel systems that emplaced the smaller, thinner, dark, smooth flows. In this scenario, the flow types could have been derived from the same magma sources, and higher flow rates would have caused disruption of the flow surface and an increase in viscosity sufficient to generate a different emplacement style in some locations.

The dark, smooth flow type exhibits morphologic properties attributed to flow inflation. Steep-sided and sometimes terraced margins, the occurrence of digitate breakout lobes, and the presence of smooth-surfaced plateaus along lava channel/tube systems indicate morphologic similarities to inflation signatures in terrestrial pahoehoe flows (e.g., Chitwood, 1994; Hon et al., 1994; Giacomini et al., 2009; Garry et al., 2012; Orr et al., 2015). Flow inflation in terrestrial environments commonly occurs for basaltic lavas in low-slope settings, in tube-fed flow units, and in relatively low-viscosity lava types when two or more are present (i.e., in pahoehoe flows in flow fields with a'a and pahoehoe present). Low emplacement rates for the breakout lobes are likely given their inferred sources in inflation plateaus; this, combined with their digitate morphology suggests that they may be analogous to small, low supply-rate compound flow lobes with pahoehoe flow textures observed at Hawaiian volcanoes (e.g., Swanson, 1973; Rowland and Walker, 1990; Hon et al., 1994; Crown and Baloga, 1999).

Observations of the sinuosity and lobate nature of the fronts and margins of dark, smooth flows and interactions with rugged flows support the interpretation of the dark, smooth flows as having a lower viscosity. Both primary emplacement morphologies (i.e., lobate flow fronts) and modified morphologies are indicated by the characteristics of the dark, smooth flows. The dark flows appear to be more fluid in nature based on their response to topographic elements of the bright rugged flows, including their margins and surface features. Complex modification of dark flow margins may be due to flow inflation and superposition of flow textures (as discussed in Section 5.2).

6.3. Terrestrial analogues

The array and diversity of volcanic morphologies observed in the extensive flow fields southwest of Arsia Mons and in northeast Daedalia Planum are similar to those found on the flanks of terrestrial basaltic shield volcanoes (e.g., Holcomb, 1987; Swanson et al., 1979). The flanks of Hawaiian shield volcanoes are characterized by a'a and pahoehoe flow textures that distinguish high- and low-viscosity flow types. The downslope morphologic zonation within individual large, rugged flows and development of prominent medial channel and levee systems southwest of Arsia Mons are generally similar to Hawaiian basaltic flows that are dominated by a'a flow textures (e.g., Wolfe, 1988; Peitersen and Crown, 1999). Lower viscosity, dark, smooth lavas that are transported through complex distributary systems composed of channels, tubes, and inflation plateaus engender comparisons to compound Hawaiian flows that exhibit pahoehoe flow textures.

Please cite this article as: Crown, D.A., Ramsey, M.S., Morphologic and thermophysical characteristics of lava flows southwest of Arsia Mons, Mars, J. Volcanol. Geotherm. Res. (2016), http://dx.doi.org/10.1016/j.jvolgeores.2016.07.008

The flow types recognized on Mars are consistent with channel-fed and tube-fed units described in previous work (Bleacher et al., 2007a, b) that showed consistent embayment of tube-fed flows by channel-fed flows on the main flanks of Arsia Mons but less consistent relationships in the plains to the south. Interactions between the flow types include deflection of the flow path for the dark, smooth lava by the locally high-standing topography of the flow fronts and margins of bright, rugged flows, as well as the their rugged surface textures. In addition, dark, smooth flows are captured by local topographic lows (i.e., central channels) within bright, rugged lobes. Based on observations presented herein and revealed through geologic mapping (Crown et al., 2015), the bright, rugged and dark, smooth flow types are intermingled both spatially and temporally within this part of the SW Arsia/NE Daedalia flow field. These complex relationships are suggestive of the interactions between pahoehoe and a'a flows on Hawaiian volcanoes. At Kilauea Volcano for example, lower viscosity, tube-fed pahoehoe lobes are commonly observed to inundate previously-emplaced pahoehoe units and to surround, invade, and sometime bury larger, thicker lobes with a'a flow textures, surmounting topographic obstacles through inflation (e.g., Crown et al., 2005). Some Hawaiian flows are also observed to undergo a downslope transition from pahoehoe to a'a, resulting in superposition of a'a flow lobes over pre-existing pahoehoe surfaces (e.g., Peterson and Tilling, 1980).

Although the identification of two intermingled flow types yields general analogies to Hawaiian basaltic flow fields, there are both important similarities and differences between the Martian and terrestrial flow fields. The morphologic characteristics of and differences between the dark, smooth and bright, rugged flow types, evidence for their low- and high-viscosity flow behavior (respectively), and the local stratigraphic relationships observed show strong similarities to Hawaiian flow fields composed of tube-fed pahoehoe and a'a flows. Furthermore, the identification of a low-viscosity lava type that is transported for long distances through insulated conduits, has a tendency to inflate, and extends from distal distributary features (including inflation plateaus) as small lobes with digitate morphology suggests that the dark, smooth flows behave in a similar fashion to terrestrial pahoehoe. However, it is important to note several potential discrepancies in the Martian-Hawaiian analogy. The Martian flows analyzed in this study are larger than typical terrestrial counterparts. The bright, rugged lobes in particular are typically longer (100 km and longer) and appear to be thicker than terrestrial lava flows. The lengths of lava flows in Hawaii are in some cases limited by their points of ocean entry. Flows from Episodes 1–20 of the Pu'u' O'o eruption of Kilauea Volcano had mean lengths of ~5 km, with maximum lengths up to 13.5 km, and thicknesses of up to 11 m (e.g., Wolfe, 1988; Peitersen and Crown, 1999). Paired a'a and pahoehoe flows from the 1859 eruption of Mauna Loa both reached the coast at distances >50 km (e.g., Greeley, 1987). Lava tubes have contributed to emplacement of the some of the longest lava flows on Earth, including flows in north Queensland (Australia) that extend to 160 km in length (Stephenson et al., 1998). Martian rugged flow surfaces also show massive bedrock outcrops rather than the rubbly surfaces of terrestrial a'a flows and do not exhibit obvious downflow textural transitions (i.e., pahoehoe to a'a). The features observed along the distributary systems for the dark, smooth flows are also larger than typical terrestrial lava tubes and inflation plateaus. Terrestrial inflation features, such as tumuli, pressure ridges, and pressure plateaus, typically show relief of 5 to 20 m (Chitwood, 1994; Hon et al., 1994). The digitate breakout lobes on Mars identified in the study area extend up to ~1 km from the bases of their inferred sources, whereas tube-fed pahoehoe lobes at the margins and within the interior of Hawaiian flow fields can be quite small with limited supply (i.e., several meters in length), but individual compound lobes have also be traced for much larger distances (i.e., many hundreds of meters) on the surfaces of the Mauna Ulu and Pu'u' O'o flow fields at Kilauea Volcano. The large difference in age between the Martian and Hawaiian flows could be responsible for some of these discrepancies. Any glassy upper surface crusts that may have existed on Mars would have been eroded over the long time period since flow emplacement. Although such factors as scale differences, flow composition, and small-scale surface characteristics require further research, the current study has documented the development of a Martian lava flow field that shows two dominant flow types, with lower and higher viscosity end-members having emplacement scenarios and interactions analogous to pahoehoe and a'a flows in terrestrial settings. These similarities do not strictly mean that a'a and pahoehoe flows, as defined for basaltic flows on the Earth, occur on Mars, but they illustrate comparable patterns in flow field development. The bright, rugged flows could be massive, blocky flows that represent the high-viscosity, a'a-like flow type, with the dark, smooth flows being the Martian pahoehoe-equivalent. Further research is needed to explore the full extent of the vast flow fields southwest of Arsia Mons and to interpret flow field development in terms of the long-term evolution of the Tharsis volcanic province.

7. Conclusions

The extensive lava flow field in our SW Arsia Mons/NE Daedalia Planum study area (22.5–27.5°S, 120–130°W) was investigated using a combination of VNIR and TIR image datasets. CTX and THEMIS images along with THEMIS-derived thermophysical and spectral properties were used to examine flow morphology, flow interactions and flow field stratigraphy, and the effects of aeolian activity on flow surfaces, as well as the spectral and thermophysical characteristics of individual lava flows. Results include:

1) The high spatial resolution of CTX images has been shown to be useful for identification and characterization of two main types of lava flows (bright, rugged flows and dark, smooth flows) that dominate the flow field southwest of Arsia Mons.
2) Bright, rugged flows have elongate sinuous planform shapes, knobby, ridged, and/or platy surface textures, are generally longer and thicker relative to dark, smooth flows, commonly display medial channel and levee systems, and may have broad distal lobes. Bright, rugged flow lobes exhibit lengths of 100 km or more in the study area and are typically 3 to 10 km wide.
3) Dark, smooth flows have relatively featureless surfaces, are typically shorter and thinner relative to bright, rugged flows, are directly associated with distributary systems that may include narrow lava channels, lava tubes, and/or sinuous ridges and plateaus. Steep-sided and sometimes terraced margins, the occurrence of digitate breakout lobes, and the presence of smooth-surfaced plateaus along lava channel/tube systems are interpreted as signatures of flow inflation. Channel segments within dark, smooth flows are typically 5 to 40 km long.
4) The smoother upper surfaces, thinner, more numerous, smaller lobes, and the channel-/tube-fed nature of the dark, smooth lava type indicates a lower viscosity lava than for the bright, rugged flows. This is consistent with interactions between the flow types and observations of dark, smooth lava inundating the surfaces of rugged flows to various degrees.
5) CTX images also reveal flow patterns and local interfingering and overlapping relationships that allow reconstruction of the complex flow field surfaces. Darker channel-/tube-fed flows are generally younger than adjacent thicker, bright, rugged flows; however, this is not always the case. The observed diversity and complexity of interactions between flows suggests that lava sources with different eruptive styles and magnitudes and/or lavas that experienced different local emplacement conditions were active contemporaneously.
6) CTX and HiRISE images of the same region show that flow field surfaces are dominated by three main types of materials: bedrock outcrops of lava, fine-grained aeolian deposits that accumulate locally in low-lying areas, and small patches of lithified, degraded TARs.

Please cite this article as: Crown, D.A., Ramsey, M.S., Morphologic and thermophysical characteristics of lava flows southwest of Arsia Mons, Mars, J. Volcanol. Geotherm. Res. (2016), http://dx.doi.org/10.1016/j.jvolgeores.2016.07.008

7) Comparisons between daytime and nighttime TIR data do not show typical temperature changes associated with surfaces dominated by either fine-grained or blocky materials. Some flow surfaces show no temperature change over a diurnal cycle, whereas, adjacent flows show both types of temperature inversion (i.e., warm during the day/cool at night and cool during the day/warm at night). This varied thermal behavior on such small spatial scales and confined to individual lava flows in some cases is attributed to the complex thermal interplay of fine-grained materials mantling, and in places infilling, rugged lava flow surfaces, with albedo effects having strong influences on the radiant temperature.
8) The TES-derived albedo (0.24–0.26) and dust cover index (0.95–0.97) predict moderate levels of dust cover in this region southwest of Arsia Mons. Some of the observed spectral contrast is attributed to variable amounts of dust cover. Flows with the lowest dust cover index and largest spectral contrast show the expected day-night temperature behavior (cool in the day/warm at night), indicating that the dust cover is optically thin (if present at all). The dominant spectral signature suggests a basaltic composition for the flows, which is consistent with the geomorphic analysis and indicates that these flows are similar to pahoehoe and a'a flows on Earth. Other spectral and thermophysical variations correlate to specific morphologic differences within, along, and across individual flows. There are certain locations where the spectral character may shift to what could be interpreted as a slightly more evolved lava composition. This could indicate changes in the erupted lava type during emplacement of the flow field or it may simply be the result of changes in the percentage of lava versus aeolian mantling material on these surfaces. Regardless, the ability to extract meaningful spectral and thermophysical information of a region generally considered inaccessible to TIR data analysis on Mars is significant and suggests that regions of Mars that have heretofore been overlooked warrant further TIR analysis.

Our initial results using THEMIS data for the southwest Arsia Mons region presented here demonstrate the utility of integrating thermophysical response and spectral variability with morphologic studies in analyses of volcanic terrains on Mars. Detailed and more comprehensive analyses of the thermophysical and spectral variations of Martian lava flow fields are ongoing (see Simurda et al., 2015) and necessary to systematically explore and fully interpret the observations presented herein. These studies should provide important constraints on both the volcanic and aeolian geology of the southern Tharsis region.

This study is one of a broader suite of geologic analyses of the southern Tharsis region of Mars, including geologic and flow field mapping of the current study area and adjacent regions (e.g., Giacomini et al., 2012; Crown et al., 2013, 2015; Garry et al., 2014), analyses of lava flow morphology and constraints on flow emplacement styles (e.g., Crown et al., 2009, 2010), and exploration of the thermophysical and spectral characteristics of Martian lava flows, including systematic comparisons of different flows and rigorous evaluations of down- and across flow variations (e.g., Ramsey and Crown, 2010; Ramsey et al., 2012; Simurda et al., 2015). This research establishes a foundation for evaluating the nature, chronology, and diversity of volcanism in the largest volcanic province on Mars.

Acknowledgements

This research was supported by NASA grants from the Mars Data Analysis Program (NNX12AJ42G) and Planetary Geology and Geophysics Program (NNX11AP56G and NNX11AP17G). The authors acknowledge Dan Berman for GIS support and helpful discussions regarding this research. Insightful reviews provided by Jacob Bleacher and Scott Rowland improved the content and presentation of this research.

References

Bandfield, J.L., 2002. Global mineral distributions on Mars. J. Geophys. Res. 107. http://dx.doi.org/10.1029/2001JE001510.
Bandfield, J.L., 2009. Effects of surface roughness and graybody emissivity on Martian thermal infrared spectra. Icarus 202. http://dx.doi.org/10.1016/j.icarus.2009.03.031.
Bandfield, J.L., Hamilton, V.E., Christensen, P.R., McSween Jr., H.Y., 2004. Identification of quartzofeldspathic materials on Mars. J. Geophys. Res. 109, E10009. http://dx.doi.org/10.1029/2004JE002290.
Bleacher, J.E., Greeley, R., Williams, D.A., Cave, S.R., Neukum, G., 2007a. Trends in effusive style at the Tharsis Montes, Mars, and implications for the development of the Tharsis province. J. Geophys. Res. 112. http://dx.doi.org/10.1029/2006JE002873.
Bleacher, J.E., Greeley, R., Williams, D.A., Werner, S.C., Hauber, E., Neukum, G., 2007b. Olympus Mons, Mars: Inferred changes in Late Amazonian aged effusive activity from lava flow mapping of Mars Express High Resolution Stereo Camera data. J. Geophys. Res. 112, E04003. http://dx.doi.org/10.1029/2006JE002826.
Bleacher, J.E., Orr, T.R., de Wet, A.P., Zimbelman, J.R., Hamilton, C.W., Garry, W.B., Crumpler, L.S., Williams, D.A., 2016. Plateaus and sinuous ridges as the fingerprints of lava flow inflation in the eastern Tharsis plains of Mars. J. Volcanol. Geotherm. Res. this volume (in review).
Bruno, B.C., Taylor, G.J., Rowland, S.K., Baloga, S.M., 1994. Quantifying the effect of rheology on lava-flow margins using fractal geometry. Bull. Volc. 56, 193–206.
Carr, M.H., Greeley, R., Blasius, K.R., Guest, J.E., Murray, J.B., 1977. Some Martian volcanic features as viewed from the Viking Orbiters. J. Geophys. Res. 82, 3985–4015.
Chitwood, L.A., 1994. Inflated basaltic lava—examples of processes and landforms from central and southeast Oregon. Or. Geol. 56, 11–20.
Christensen, P.R., 1982. Martian dust mantling and surface composition: interpretation of thermophysical properties. J. Geophys. Res. 87, 9985–9998. http://dx.doi.org/10.1029/JB087iB12p09985.
Christensen, P.R., et al., 2004. Mineralogy at Meridiani Planum from the mini-TES experiment on the opportunity rover. Science 306, 1733–1739. http://dx.doi.org/10.1126/science.1104909.
Chuang, F.C., Crown, D.A., Tornabene, L.L., 2015. Zumba crater, Daedalia Planum, Mars: geologic investigation of a young, rayed impact crater and its secondary field. Icarus 269, 75–90. http://dx.doi.org/10.1016/j.icarus.2016.01.005.
Crown, D.A., 2016. Geologic Map of MTM -25127 and -25122 Quadrangles, Daedalia Planum Region of Mars. U.S. Geological Survey (in preparation).
Crown, D.A., Baloga, S.M., 1999. Pahoehoe toe dimensions, morphology and branching relationships at Mauna Ulu, Kilauea Volcano, Hawaii. Bull. Volcanol. 61, 288–305.
Crown, D.A., Berman, D.C., 2012. Geologic mapping of MTM -35137 quadrangle: Daedalia Planum region of Mars. Lunar and Planetary Science Conference XLIII, Abstract 2055. Houston, Lunar and Planetary Institute.
Crown, D.A., Anderson, S.W., Byrnes, J.M., Ramsey, M.S., 2005. Distributary systems in basaltic flow fields: insights from Mauna Ulu, Kilauea Volcano, Hawaii. EOS Trans. AGU, Fall Meet. Suppl., Abstract V53B-1564.
Crown, D.A., Berman, D.C., Rivas, R., Ramsey, M.S., 2009. Arsia Mons lava flows: insights into flow field emplacement and stratigraphy from CTX and HiRISE images. Lunar and Planetary Science Conference XL, Abstract 2252. Lunar and Planetary Institute, Houston.
Crown, D.A., Ramsey, M.S., Berman, D.C., 2010. Mapping Arsia Mons lava flow fields: insights into flow emplacement processes and flow field development. Lunar and Planetary Science Conference XLI, Abstract 2225. Lunar and Planetary Institute, Houston.
Crown, D.A., Ramsey, M.S., Berman, D.C., 2011. Lava flow fields of southern Tharsis, Mars: mapping, morphologic, and chronologic studies. Lunar and Planetary Science Conference XLII, Abstract 2352. Lunar and Planetary Institute, Houston.
Crown, D.A., Ramsey, M.S., Berman, D.C., 2012. Morphologic and chronologic studies of lava flow fields in the southern Tharsis region of Mars. Lunar and Planetary Science Conference XLIII, Abstract 2138. Lunar and Planetary Institute, Houston.
Crown, D.A., Berman, D.C., Chuang, F.C., 2013. Geologic mapping of the southern extent of Tharsis volcanism in MTM -35137 quadrangle, Daedalia Planum, Mars. Lunar and Planetary Science Conference XLIV, Abstract 2499. Lunar and Planetary Institute, Houston.
Crown, D.A., Berman, D.C., Ramsey, M.S., 2015. Lava flow fields of southern Tharsis, Mars: flow types, interactions, and ages. Lunar and Planetary Science Conference XLVI, Abstract 1439. Lunar and Planetary Institute, Houston.
Crown, D.A., Berman, D.C., Chuang, F.C., 2016. Geologic map of MTM -35137 quadrangle. Daedalia Planum Region of Mars. U.S. Geological Survey (in preparation).
Crumpler, L.S., Aubele, J.C., 1978. Structural evolution of Arsia Mons, Pavonis Mons, and Ascraeus Mons: Tharsis region of Mars. Icarus 34, 496–511.
Crumpler, L.S., Head, J.W., Aubele, J.C., 1996. Calderas on Mars: characteristics, structure and associated flank deformation. In: McGuire, W.J., Jones, A.P., Neuberg, J. (Eds.), Volcano Instability on the Earth and Other Planets. Geol. Soc. Spec. Publ. 110, pp. 307–348.
Dohm, J.M., Tanaka, K.L., Hare, T.M., 2001. Geologic, paleotectonic, and paleoerosional maps of the Thaumasia region, Mars. U.S. Geol. Surv. Geol. Invest. Ser. Map I-2650.
Edwards, C.S., Nowicki, K.J., Christensen, P.R., Hill, J., Gorelick, N., Murray, K., 2011. Mosaicking of global planetary image datasets: 1. Techniques and data processing for thermal emission imaging system (THEMIS) multi-spectral data. J. Geophys. Res. 116, E10008. http://dx.doi.org/10.1029/2010JE003755.
Fergason, R.L., Christensen, P.R., Kieffer, H.H., 2006. High-resolution thermal inertia derived from the thermal emission imaging system (THEMIS): thermal model and applications. J. Geophys. Res. 111, E12004. http://dx.doi.org/10.1029/2006JE002735.
Fink, J.H., Zimbelman, J.R., 1990. Longitudinal variations in rheological properties of lavas: Puu Oo basalt flows, Kilauea Volcano, Hawaii. In: Fink, J.H. (Ed.), Lava Flows and Domes: Emplacement Mechanisms and Hazard Implications. Springer-Verlag, New York (249 pp.).

Please cite this article as: Crown, D.A., Ramsey, M.S., Morphologic and thermophysical characteristics of lava flows southwest of Arsia Mons, Mars, J. Volcanol. Geotherm. Res. (2016), http://dx.doi.org/10.1016/j.jvolgeores.2016.07.008

Garry, W.B., Robinson, M.S., Zimbleman, J.R., Bleacher, J.E., Hawke, B.R., Crumpler, L.S., Braden, S.E., Sato, H., 2012. The origin of Ina: evidence for inflated lava flows on the Moon. J. Geophys. Res. 117. http://dx.doi.org/10.1029/2011JE003981.

Garry, W.B., Williams, D.A., Bleacher, J.E., 2014. Geologic mapping of Arsia and Pavonis Montes, Mars. Lunar and Planetary Science Conference XLV. Lunar and Planetary Institute, Houston (Abstract 2133).

Giacomini, L., Massironi, M., Martellato, E., Pasquare, G., Firgeri, A., Cremonese, G., 2009. Inflated flows on Daedalia Planums (Mars)? Clues from a comparative analysis with the Payen volcanic complex (Argentina). Planet. Space Sci. 57, 556–570.

Giacomini, L., Carli, C., Sgavetti, M., Massironi, M., 2012. Spectral analysis and geological mapping of the Daedalia Planum lava field (Mars) using OMEGA data. Icarus 220, 679–693.

Gillespie, A.R., 1992. Enhancement of multispectral thermal infrared images: decorrelation contrast stretching. Remote Sens. Environ. 42, 147–155.

Glaze, L.S., Baloga, S.M., Garry, W.B., Fagents, S.A., Parcheta, C., 2009. A hybrid model for leveed lava flows: implications for eruption styles on Mars. J. Geophys. Res. 114. http://dx.doi.org/10.1029/2008JE003278.

Greeley, R., 1987. The role of lava tubes in Hawaiian volcanoes. U.S. Geol. Surv. Prof. Paper 1350, 1589–1602.

Head, J.W., Siebert, N., Pratt, S., Smith, D., Zuber, M., Garvin, J.B., McGovern, P.J., the MOLA Science Team, 1998a. Volcanic calderas on Mars: initial views using Mars Orbiter Laser Altimeter (MOLA) data. Lunar and Planetary Science Conference XXIX (Abstract 1488).

Head, J.W., Siebert, N., Pratt, S., Smith, D., Zuber, M., Solomon, S., McGovern, P.J., Garvin, J.B., the MOLA Science Team, 1998b. Characterization of major volcanic edifices on Mars using Mars Orbiter Laser Altimeter (MOLA) data. Lunar and Planetary Science Conference XXIX (Abstract 1322).

Holcomb, R.T., 1987. Eruptive history and long-term behavior of Kilauea Volcano. U.S. Geol. Surv. Prof. Paper 1350, 261–350.

Holmok, S., 2012. Pilot Study for the Determination of Eruption Rates in the Tharsis Region (Mars) Based on Mapping and Age Determinations of Lava Flows. Unpublished B·Sc. thesis, Freie Universität Berlin, Berlin, 23p. (in German)

Hon, K., Kauahikaua, J., Denlinger, R., Mackay, K., 1994. Emplacement and inflation of pahoehoe sheet flows: observations and measurements of active lava flows on Kilauea Volcano, Hawaii. Geol. Soc. Am. Bull. 106, 351–370.

Hulme, G., 1974. The interpretation of lava flow morphology. Geophys. J. R. Astron. Soc. 39, 361–383.

Kapannusch, R., 2012. Mapping and Age Determinations of Selected Lava Flows in Daedalia Planum (Mars) - Basic Concept for Determining Eruption Rates in the Tharsis Region. Unpublished B·Sc. thesis, Freie Universität Berlin, Berlin, 24p. (in German)

Lang, N.P., Tornabene, L.L., McSween, H.Y., Christensen, P.R., 2009. Tharsis-sourced relatively dust-free lavas and their possible relationship to Martian meteorites. J. Volc. Geotherm. Res. 185, 103–115.

Lopes, R.M.C., Kilburn, C.R.J., 1990. Emplacement of lava flow fields: application of terrestrial studies to Alba Patera, Mars. J. Geophys. Res. 95, 14383–14397.

Moore, H.J., Arthur, D.W.G., Schaber, G.G., 1978. Yield strengths of flows on Earth, Moon, and Mars. Proc. Lunar Planet. Sci. Conf., 9th, pp. 3351–3378.

Mouginis-Mark, P.J., 2002. Prodigious ash deposits near the summit of Arsia Mons volcano, Mars. Geophys. Res. Lett. 29, 1768. http://dx.doi.org/10.1029/2002GL015296.

Orr, T.R., Bleacher, J.E., Patrick, M.R., Wooten, K.M., 2015. A sinuous tumulus over an active lava tube at Kilauea Volcano: evolution, analogs, and hazard forecasts. J. Volcanol. Geotherm. Res. 291, 35–48.

Peitersen, M.N., Crown, D.A., 1999. Downflow width behavior of Martian and terrestrial lava flows. J. Geophys. Res. 104, 8473–8488.

Peterson, D.W., Tilling, R.I., 1980. Transition of basaltic lava from pahoehoe to aa, Kilauea Volcano, Hawaii: field observations and key factors. J. Volcanol. Geotherm. Res. 7, 271–293.

Plescia, J.B., 2004. Morphometric properties of Martian volcanoes. J. Geophys. Res. 109, E03003. http://dx.doi.org/10.1029/2002JE002031.

Price, M.A., Ramsey, M.S., Crown, D.A., 2013. Thermophysical characteristics of mantled terrestrial volcanic surfaces: infrared analogs to the Arsia Mons flows. Lunar and Planetary Science Conference XLIV. Lunar and Planetary Institute, Houston (Abstract 1640).

Ramsey, M.S., Christensen, P.R., 1998. Mineral abundance determination: quantitative deconvolution of thermal emission spectra. J. Geophys. Res. 103, 577–596.

Ramsey, M.S., Crown, D.A., 2010. Thermophysical and spectral variability of Arsia Mons lava flows. Lunar and Planetary Science Conference XLI. Lunar and Planetary Institute, Houston (Abstract 1111).

Ramsey, M.S., Fink, J.H., 1999. Estimating silicic lava vesicularity with thermal remote sensing: a new technique for volcanic mapping and monitoring. Bull. Volcanol. 61, 32–39.

Ramsey, M.S., Crown, D.A., Price, M.A., 2012. Decoupling lava flow composition and emplacement processes from eolian mantling deposits using thermal infrared data. Lunar and Planetary Science Conference XLIII. Lunar and Planetary Institute, Houston (Abstract 2013).

Realmuto, V.J., 1990. Separating the effects of temperature and emissivity: emissivity spectrum normalization. In: Abbott, E.A. (Ed.), Proceedings of the 2nd TIMS Workshop. Jet Propulsion Laboratory, Pasadena, pp. 31–37.

Rose, S.R., Watson, I.M., Ramsey, M.S., Hughes, C.G., 2014. Thermal deconvolution: accurate retrieval of multispectral infrared emissivity from thermally-mixed volcanic surfaces. Remote Sens. Environ. 140, 690–703. http://dx.doi.org/10.1016/j.rse.2013.10.009.

Rowland, S.K., Walker, G.P.L., 1990. Pahoehoe and aa in Hawaii: volumetric flow rate controls the lava structure. Bull. Volcanol. 52, 615–628.

Rowland, S.K., Harris, A.J.L., Garbeil, H., 2004. Effects of Martian conditions on numerically modeled, cooling-limited channelized lava flows. J. Geophys. Res. 109. http://dx.doi.org/10.1029/2004JE002288.

Ruff, S.W., Christensen, P.R., 2002. Bright and dark regions on Mars: particle size and mineralogical characteristics based on thermal emission spectrometer data. J. Geophys. Res. 107. http://dx.doi.org/10.1029/2001JE001580.

Schaber, G.G., Horstman, K.C., Dial, A.L., 1978. Lava flow materials in the Tharsis region of Mars. Proc. Lunar Planet. Sci. Conf., 9th, pp. 3433–3458.

Scott, D.H., 1981. Map showing lava flows in the southeast part of the Phoenicis Lacus quadrangle of Mars. U.S. Geol. Surv. Misc. Invest. Ser. Map I-1274, Scale 1:2 M.

Scott, D.H., Tanaka, K.L., 1981. Map showing lava flows in the northeast part of the Phaethontis quadrangle of Mars. U.S. Geol. Surv. Misc. Invest. Ser. Map I-1281, Scale 1:2 M.

Scott, D.H., Tanaka, K.L., 1986. Geologic map of the western equatorial region of Mars. U.S. Geol. Surv. Misc. Invest. Map I-1802-A, Scale 1:15 M.

Scott, D.H., Zimbelman, J.R., 1995. Geologic map of Arsia Mons volcano, Mars. U.S. Geol. Surv. Geol. Series Map I-2480, Scale 1:1 M.

Scott, D.H., Shaber, G.G., Dial, A.L., 1981. Map showing lava flows in the southwest part of the Phoenicus Lacus quadrangle of Mars. U.S. Geol. Surv. Misc. Invest. Ser. Map I-1275, Scale 1:2 M.

Simurda, C.M., Ramsey, M.S., Crown, D.A., 2015. Thermophysical characteristics of lava flows south of Arsia Mons. Lunar and Planetary Science Conference XLVI. Lunar and Planetary Institute, Houston (Abstract 2332).

Stephenson, P.J., Burch-Johnston, A.T., Stanton, D., Whitehead, P.W., 1998. Three long lava flows in north Queensland. J. Geophys. Res. 103, 27,359–27,370.

Swanson, D.A., 1973. Pahoehoe flows from the 1969–1971 Mauna Ulu eruption, Kilauea Volcano, Hawaii. Geol. Soc. Am. Bull. 84, 615–626.

Swanson, D.A., Duffield, W.A., Jackson, D.B., Peterson, D.W., 1979. Chronological narrative of the 1969–1971 Mauna Ulu eruption of Kilauea Volcano, Hawaii. U.S. Geol. Surv. Prof. Paper 1056, 1–55.

Walker, G.P.L., 1991. Structure, and origin by injection of lava under surface crust, of tumuli, "lava rises", "lava-rise pits", and "lava-inflation clefts", in Hawaii. Bull. Volcanol. 53, 546–558.

Warner, N.H., Gregg, T.K.P., 2003. Evolved lavas on Mars? Observations from southwest Arsia Mons and Sabancaya volcano. Peru. J. Geophys. Res. 108. http://dx.doi.org/10.1029/2002JE001969.

Whitehead, P.W., Stephenson, P.J., 1998. Lava rise ridges of the Toomba basalt flow, north Queensland, Australia. J. Geophys. Res. 103, 27,371–27,382.

Wolfe, E.W. (Ed.), 1988. The Puu Oo eruption of Kilauea Volcano, Hawaii: episodes 1 through 20, January 3, 1983, through June 8, 1984. U.S. Geol. Surv. Prof. Paper 1463.

Please cite this article as: Crown, D.A., Ramsey, M.S., Morphologic and thermophysical characteristics of lava flows southwest of Arsia Mons, Mars, J. Volcanol. Geotherm. Res. (2016), http://dx.doi.org/10.1016/j.jvolgeores.2016.07.008